Comprehensive validation of an intermittency transport model for transitional low-pressure turbine flows

Y. B. Suzen and P. G. Huang
Department of Mechanical Engineering
University of Kentucky
USA

ABSTRACT

A transport equation for the intermittency factor is employed to predict transitional flows under the effects of pressure gradients, freestream turbulence intensities, Reynolds number variations, flow separation and reattachment, and unsteady wake–blade interactions representing diverse operating conditions encountered in low-pressure turbines. The intermittent behaviour of the transitional flows is taken into account and incorporated into computations by modifying the eddy viscosity, μ_τ, with the intermittency factor, γ. Turbulent quantities are predicted by using Menter's two-equation turbulence model (SST). The onset location of transition is obtained from correlations based on boundary-layer momentum thickness, accelaration parameter, and turbulence intensity. The intermittency factor is obtained from a transport model which can produce both the experimentally observed streamwise variation of intermittency and a realistic profile in the cross stream direction.

The intermittency transport model is tested and validated against several well documented low pressure turbine experiments ranging from flat plate cases to unsteady wake–blade interaction experiments. Overall, good agreement between the experimental data and computational results is obtained illustrating the predicting capabilities of the model and the current intermittency transport modelling approach for transitional flow simulations.

NOMENCLATURE

C_p	pressure coefficient, $2(P - P_\infty)/(\rho_\infty U_{in}^2)$
C_x	axial chord
FSTI	freestream turbulence intensity (%)
k	turbulent kinetic energy
K_t	flow acceleration parameter, $(\nu/U^2)(dU/ds)$
L_x	axial chord
n	spot generation rate
N	non-dimensional spot breakdown rate parameter, $n\sigma\theta_t^3/\nu$
P	static pressure
P_{total}	total pressure
Re	Reynolds number
Re_{st}	$(s_t - s_s)U_e/\nu$
$Re_{\theta t}$	$\theta_t U_e/\nu$
s	streamwise distance along suction surface
Tu	turbulence intensity (%), u'/U
u_τ	friction velocity
U	boundary-layer streamwise velocity
U_e	local freestream velocity
U_{in}	inlet freestream velocity
W	magnitude of vorticity
y_n	distance normal to the wall
y^+	$y_n u_\tau/\nu$
γ	intermittency factor
θ	momentum thickness
λ_θ	pressure gradient parameter, $(\theta^2/\nu)(dU/ds)$
μ	molecular viscosity
μ_t	eddy viscosity
μ	μ/ρ
ν_t	μ_t/ρ
ρ	density
σ	spot propagation parameter

Paper No. 2889. Manuscript received 7 April 2004, revised version received 26 October 2004, accepted 1 December 2004.

https://doi.org/10.1017/S0001924000000610 Published online by Cambridge University Press

Subscripts

e freestream
s onset of separation
t onset of transition

1.0 INTRODUCTION

Flows in low-pressure turbines involve complex interplays of several physical mechanisms such as laminar or turbulent flow separation, wake/boundary-layer interactions, and flow transition. At a given instant the boundary layer over a low-pressure turbine blade may experience one or more modes of transition including bypass transition, separated flow transition, wake-induced periodic transition, and relaminarisation. These transitional flows are affected by freestream turbulence, diverse pressure gradients, wide range of Reynolds numbers, flow separation, and unsteady wake–boundary-layer interactions. Accurate prediction of this type of complex flows has great importance in design of more efficient jet engines.

In low pressure turbines, unpredicted losses and substantial drops in efficiency have been observed at high altitudes and cruise speeds which correspond to low Reynolds number conditions[1-3]. These drops in efficiency and increase in fuel consumption are direct consequences of flow separation on the suction side of the turbine blades. At low Reynolds number conditions the flow over the blades is essentially laminar and susceptible to separation on the aft part of the suction surface due to adverse pressure gradients. For Reynolds numbers lower than 200,000, nearly 300% rise in loss coefficients were observed due to flow separation[4]. In order to calculate the losses and heat transfer on various components of gas turbine engines, and to be able to improve component efficiencies and reduce losses through better designs, accurate prediction of development of transitional boundary layers is essential[1].

In modelling transitional flows one successful approach is to incorporate the concept of intermittency into computations. This can be done by multiplying the eddy viscosity obtained from a turbulence model, μ_t, used in the diffusive parts of the mean flow equations, by the intermittency factor[5], γ. This method can be easily incorporated into any Reynolds Averaged Navier Stokes solver. In this approach, the intermittency factor, γ can be obtained from an empirical relation such as the generalised intermittency distribution correlation of Dhawan and Narasimha[6], improved correlations of Gostelow *et al*[7] or Solomon *et al*[8]. The effects of freestream turbulence intensity and pressure gradients on transition can be incorporated into computations by formulating intermittency distribution in terms of those parameters. Alternatively, the intermittency factor can be obtained from a transport model.

Steelant and Dick[9] developed a transport equation for intermittency, which reproduced the γ distribution of Dhawan and Narasimha[6] across the transition region. Steelant and Dick used their model, coupled with two sets of conditioned Navier-Stokes equations, to predict transitional flows with zero, favorable, and adverse pressure gradients. However, since their technique involved the solution of two sets of strongly coupled equations, the method is not compatible with existing CFD codes, in which only one set of Navier-Stokes equations is involved. Moreover, the model was designed to provide a realistic streamwise γ behaviour but with no consideration of the variation of γ in the cross-stream direction. Experimental studies indicate that the intermittency is a function of both the streamwise distance and the distance normal to the surface. The profile in cross-stream direction has a peak near the wall and decay to zero near the edge of the boundary layer[1].

The κ–ε–γ turbulence model developed by Cho and Chung[10] for free shear flows explicitly incorporates the intermittency effect into the conventional κ–ε model equations by introducing an additional transport equation for γ. They applied this model to compute a plane jet, a round jet, a plane far wake, and a plane mixing layer with good agreements. Although this method was not designed to reproduce flow transition it provided a realistic profile of γ in the cross-stream direction. In order to extend the model's superior free shear flow performance to wall bounded shear flows Drikakis and Goldberg[11] introduced a Low-Re version of the κ–ε–γ model and used the new model in computations of channel flow, flat plate flow, and flow over a slanted backward-facing step with success.

Suzen and Huang[12] developed an intermittency transport equation combining the best properties of Steelant and Dick's model and Cho and Chung's model. The model reproduces the streamwise intermittency distribution of Dhawan and Narasimha[6] and also produces a realistic variation of intermittency in the cross-stream direction. In their approach, Suzen and Huang[12] used the intermittency transport model to obtain the intermittency distribution for the transitional flows with the onset of transition defined from correlations based on momentum thickness, accelaration parameter, and turbulence intensity. Depending on whether the flow is attached or separated the onset of transition is determined using attached-flow or separated-flow transition onset correlations. Although its dependence on the boundary-layer momentum thickness limits its extension to three dimensional applications and unstructured grids, the intermittency model and the accompanying correlations have been sucessfully applied to a wide range of low-pressure turbine flows indicating that the intermittency transport modelling approach provides an accurate and practical computational tool for transitional flow simulations.

In this paper, a comprehensive overview of the validation of the intermittency transport model against a wide range of benchmark low-pressure turbine experiments is presented. The model has been validated against T3- series experiments of Savill[13,14], low-pressure turbine experiments of Simon *et al*[15] and separated and transitional boundary-layer experiments of Volino and Hultgren[16], PAK-B cascade experiments of Lake *et al*[3,17], Huang *et al*[18], Volino[19], wake–blade interaction experiments of Kaszeta *et al*[20,21], and Stieger[22] with success[12,23-30]. These experiments represent a wide range of low pressure turbine operating conditions and include effects of pressure gradients, freestream turbulence intensities, Reynolds numbers, flow separation, and unsteadiness on transition. The application of the intermittency transport model to these experiments has been described fully in literature[12,23-30] and in this paper the results have been summarised in order to provide an overall review of the predicting capabilities of the model for transitional low-pressure turbine flows.

In the next section, the intermittency transport model is presented and implementation of the model and the empirical correlations employed for the onset of transition are described. In Section 3, the results for simulations of benchmark experiments using intermittency transport model are given and conclusions are provided in Section 4.

2.0 INTERMITTENCY TRANSPORT MODEL

The model blends the transport equation models of Steelant and Dick[9] and Cho and Chung[10] into one transport equation to combine the desired properties of each model, namely the ability to produce the streamwise γ distribution of Dhawan and Narasimha[6] and to provide a realistic variation of intermittency in the cross-stream direction. Details of the development and implementation of the transport model are given in Suzen and Huang[12,23,24], Suzen *et al*[28]. The model equation is given by:

$$\frac{\partial \rho\gamma}{\partial t}+\frac{\partial \rho u_j\gamma}{\partial x_j}=$$
$$(1-\gamma)\left[\begin{array}{l}(1-F)2C_0\rho\sqrt{u_k u_k}\,f(s)f'(s)\\ +F\left(\dfrac{C_1\gamma}{k}\tau_{ij}\dfrac{\partial u_i}{\partial x_j}-C_2\gamma\rho\dfrac{k^{3/2}}{\varepsilon}\dfrac{u_i}{(u_k u_k)^{1/2}}\dfrac{\partial u_i}{\partial x_j}\dfrac{\partial \gamma}{\partial x_j}\right)\end{array}\right] \quad \ldots(1)$$
$$+C_3\rho\frac{k^2}{\varepsilon}\frac{\partial\gamma}{\partial x_j}\frac{\partial\gamma}{\partial x_j}$$
$$+\frac{\partial}{\partial x_j}\left((1-\gamma)\left(\gamma\sigma_{\gamma_L}\mu+\sigma_{\gamma_T}\mu_t\right)\frac{\partial\gamma}{\partial x_j}\right)$$

https://doi.org/10.1017/S0001924000000610 Published online by Cambridge University Press

The distributed breakdown function, $f(s)$ has the form:

$$f(s) = \frac{as'^4 + bs'^3 + cs'^2 + ds' + e}{gs'^3 + h} \quad \ldots (2)$$

where $s' = s - s_t$, and s is the distance along the streamline coordinate, and s_t is the transition location. The coefficients are;

$$a = 50\sqrt{\frac{n\sigma}{U}}$$

$$b = -0{\cdot}4906$$

$$c = 0{\cdot}204\left(\frac{n\sigma}{U}\right)^{-0{\cdot}5}$$

$$d = 0{\cdot}0 \quad \ldots (3)$$

$$e = 0{\cdot}04444\left(\frac{n\sigma}{U}\right)^{-1{\cdot}5}$$

$$h = 10e$$

$$g = 50$$

In these definitions n is the turbulent spot generation rate and σ is Emmons' dimensionless spot propagation rate.

The shear stresses are defined as:

$$\tau_{ij} = \mu_t\left[\frac{\partial u_i}{\partial x_j} + \frac{\partial u_j}{\partial x_i} - \frac{2}{3}\frac{\partial u_k}{\partial x_k}\delta_{ij}\right] - \frac{2}{3}\rho k\delta_{ij} \quad \ldots (4)$$

The blending function F is constructed using a nondimensional parameter, $k/W\nu$ where k is the turbulent kinetic energy and W is the magnitude of the vorticity. The blending function has the form:

$$F = \mathrm{Tan\,h}^4\left[\frac{k/W\nu}{200\left(1-\gamma^{0{\cdot}1}\right)^{0{\cdot}3}}\right] \quad \ldots (5)$$

The model constants used in Equation 1 are:

$$\sigma_{\gamma_L} = \sigma_{\gamma_T} = 1{\cdot}0 \quad C_0 = 1{\cdot}0 \quad C_1 = 1{\cdot}6$$
$$C_2 = 0{\cdot}16 \quad C_3 = 0{\cdot}15$$

Initially γ is set to zero throughout the flowfield. On solid wall boundaries the value of γ is kept as zero; at the freestream, a zero gradient of γ is assumed and on outflow boundaries γ is extrapolated from inside the domain to the outer boundaries.

The intermittency is incorporated into the computations simply by multiplying the eddy viscosity obtained from a turbulence model, μ_t, by the intermittency factor, γ. Simon and Stephens[5] showed that by combining the two sets of conditioned Navier-Stokes equations and making the assumption that the Reynolds stresses in the nonturbulent part are negligible, the intermittency can be incorporated into the computations by using the eddy viscosity, μ_t^* which is obtained by multiplying the eddy viscosity from a turbulence model, μ_t, with the intermittency factor, γ. That is,

$$\mu_t^* = \gamma\mu_t \quad \ldots (6)$$

is used in the mean low equations. It must be noted that γ does not appear in the generation term of the turbulent kinetic energy equations.

In using this intermittency approach, the turbulence model selected to obtain μ_t must produce fully turbulent features before transition location in order to allow the intermittency to have full control of the transitional behaviour. Menter's[31] SST model satisfies this requirement. It produces almost fully turbulent flow in the leading edge of the boundary layer and therefore it is used as a baseline model to compute μ_t and other turbulent quantities in the computations[28].

The value of $n\sigma$ used in evaluating the constants given by Equation (3) is provided by the following correlation for zero pressure gradient flows[28];

$$\hat{n}\sigma = \left(n\nu^2/U^3\right)\sigma = 1{\cdot}8\times10^{-11}Tu^{7/4} \quad \ldots (7)$$

When flows are subject to pressure gradients, the following correlation is used:

$$\frac{\hat{n}\sigma}{(\hat{n}\sigma)_{ZPG}} = \begin{cases} M^{\left(1-\exp\left(0{\cdot}75\times10^6 K_t Tu^{-0{\cdot}7}\right)\right)}, & K_t < 0 \\ 10^{-3227K_t^{0{\cdot}5985}}, & K_t > 0 \end{cases} \quad \ldots (8)$$

with M defined as:

$$M = \left(850Tu^{-3} - 100Tu^{-0{\cdot}5} + 120\right)$$

where, $(\hat{n}\sigma)_{ZPG}$ is the value for flow at zero pressure gradient and can be obtained from Equation (7) and $K_t = (\nu/U_t^2)\mathrm{d}U/\mathrm{d}x)_t$ is the flow acceleration parameter. The favourable-pressure gradient part of the above correlation (for $K_t > 0$) is from Steelant and Dick[9]. The portion of the correlation for adverse pressure gradient flows for $K_t < 0$, is formulated using the transition data of Gostelow *et al*[7] and Simon *et al*[15] in Suzen *et al*[28].

The current approach uses the intermittency transport model to obtain the intermittency distribution for the transitional flows, while the onset of transition is defined by correlations. Attached-flow transition onset correlation or separated-flow transition onset correlation is used depending on whether the flow is attached or separated. The onset of attached flow transition is determined by the following correlation in terms of turbulence intensity, Tu, and the acceleration parameter, K_t,

$$\mathrm{Re}_{\theta t} = \left(120 + 150Tu^{-2/3}\right)\mathrm{Cot\,h}\left[4\left(0{\cdot}3 - K_t\times10^5\right)\right] \quad \ldots (9)$$

where K_t was chosen as the maximum absolute value of that parameter in the downstream deceleration region[28]. This correlation maintains the good features of Abu-Ghannam and Shaw[32] correlation in the adverse pressure gradient region and in addition it reflects the fact that the flow becomes less likely to have transition when subject to favorable pressure gradients by rapidly rising as K_t becomes positive.

In order to determine the onset of separated flow transition Re_{st} is expressed in terms of the turbulence intensity (Tu) and the momentum thickness Reynolds number at the point of separation $\mathrm{Re}_{\theta s}$ in the form[27];

$$\mathrm{Re}_{st} = 874\,\mathrm{Re}_{\theta s}^{0{\cdot}71}\exp\left[-0{\cdot}4Tu\right] \quad \ldots (10)$$

This correlation provides a better representation of the experimental data than Davis *et al*[33] correlation and is used to predict onset of separated flow transition in the present computations.

The production term of the intermittency transport model requires calculation of streamwise distance. For simple blade geometries streamwise distance from transition onset point can be calculated based on blade geometry, however, for complex geometries this task may become difficult. In order to eliminate the difficulties associated with calculating the streamwise distance from geometric information alone we developed a transport equation for streamwise distance s. The derivation of the s equation is given below.

Streamwise distance s is defined as:

$$s = \int\frac{u\mathrm{d}x + v\mathrm{d}y}{\sqrt{u^2+v^2}} \quad \ldots (11)$$

https://doi.org/10.1017/S0001924000000610 Published online by Cambridge University Press

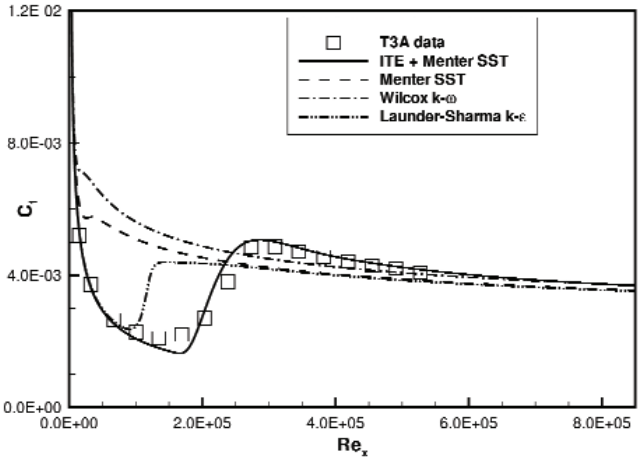


Figure 1. Comparison of skin friction coefficient for zero pressure gradient T3A case.

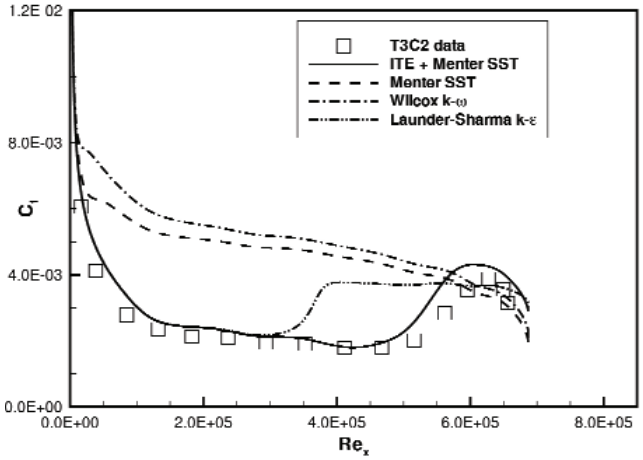


Figure 2. Comparison of skin friction coefficient for variable pressure gradient T3C2 case.

Then,

$$ds = \int \frac{u\,dx + v\,dy}{\sqrt{u^2 + v^2}} \qquad \ldots (12)$$

writing $dx = u\,dt$, $dy = v\,dt$

$$ds = \frac{u^2 + v^2}{\sqrt{u^2 + v^2}}\,dt = \sqrt{u^2 + v^2}\,dt \qquad \ldots (13)$$

simplifying, we obtain

$$\frac{ds}{dt} = \sqrt{u^2 + v^2} \qquad \ldots (14)$$

that is,

$$\frac{ds}{dt} = \frac{\partial s}{\partial t} + u\frac{\partial s}{\partial x} + v\frac{\partial s}{\partial y} = \sqrt{u^2 + v^2} \qquad \ldots (15)$$

with addition of density we have,

$$\frac{\partial \rho s}{\partial t} + u\frac{\partial \rho s}{\partial x} + v\frac{\partial \rho s}{\partial y} = \rho\sqrt{u^2 + v^2} \qquad \ldots (16)$$

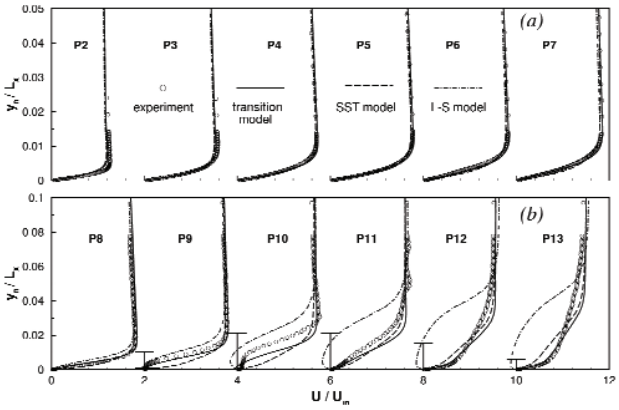


Figure 3. Comparison of velocity profiles for Re = 100,000, FSTI = 10%, transition model *vs* pure turbulence models: (a) P2-P7 stations and (b) P8-P13 stations.

In order to make the computed s values in freestream penetrate the boundary layer up to the solid walls and also to avoid accumulation of s in low speed circulating flow regions a diffusion term is included. With addition of a diffusion term, making use of continuity equation, and writing in indicial form, the equation becomes,

$$\frac{\partial(\rho s)}{\partial t} + \frac{\partial(\rho u_i s)}{\partial x_i} = \rho\sqrt{u_k u_k} + \frac{\partial}{\partial x_i}\left[\frac{(\mu + \mu_t)}{\sigma_s}\frac{\partial s}{\partial x_i}\right] \qquad \ldots (17)$$

where $\sigma_s = 0{\cdot}1$ is used.

The initial condition of $s = 0{\cdot}0$ is used all over the flow field. The gradient of s is set to zero at all boundaries.

For steady state computations once the flow field develops s changes very little and gradually, this equation is solved simultaneously with the intermittency transport equation. For time dependent computations, s equation is solved before intermittency transport equation at each time level. The changes in s are gradual from one time step to the next. The intermittency transport model uses the streamwise distance from the onset point of transition. Once the onset point of transition is calculated, the value of s at that point, s_t, is subtracted from s values of all points:

$$s' = s - s_t \qquad \ldots (18)$$

If s' is less than or equal to zero the production term of the intermittency model becomes zero, keeping flow laminar upstream of transition onset point.

Initially, the intermittency model had been implemented into TURCOM code developed by Huang and Coakley[34] and validated against low-pressure turbine experiments of Simon *et al*[15] and separated and transitional boundary-layer experiment Volino and Hultgren[16], (Suzen *et al*[26,28]). Computations of the rest of the experiments are performed using a recently developed multi-block Navier-Stokes solver, called GHOST, developed at University of Kentucky by George Huang. GHOST is a pressure-based code based on SIMPLE (semi-implicit method for pressure-linked equation) algorithm with second order accuracy in both time and space. Advection terms are approximated by a QUICK (quadratic upstream interpolation for convection kinematic) scheme and central differencing is used for the viscous terms. The 'Rhie and Chow' momentum interpolation method[35] is employed to avoid checkerboard oscillations usually associated with the non-staggered grid arrangement. This code is capable of handling complex geometries, moving, and overset grids and includes multiprocessor computation capability using MPI (message passing interface). Since multiple

https://doi.org/10.1017/S0001924000000610 Published online by Cambridge University Press

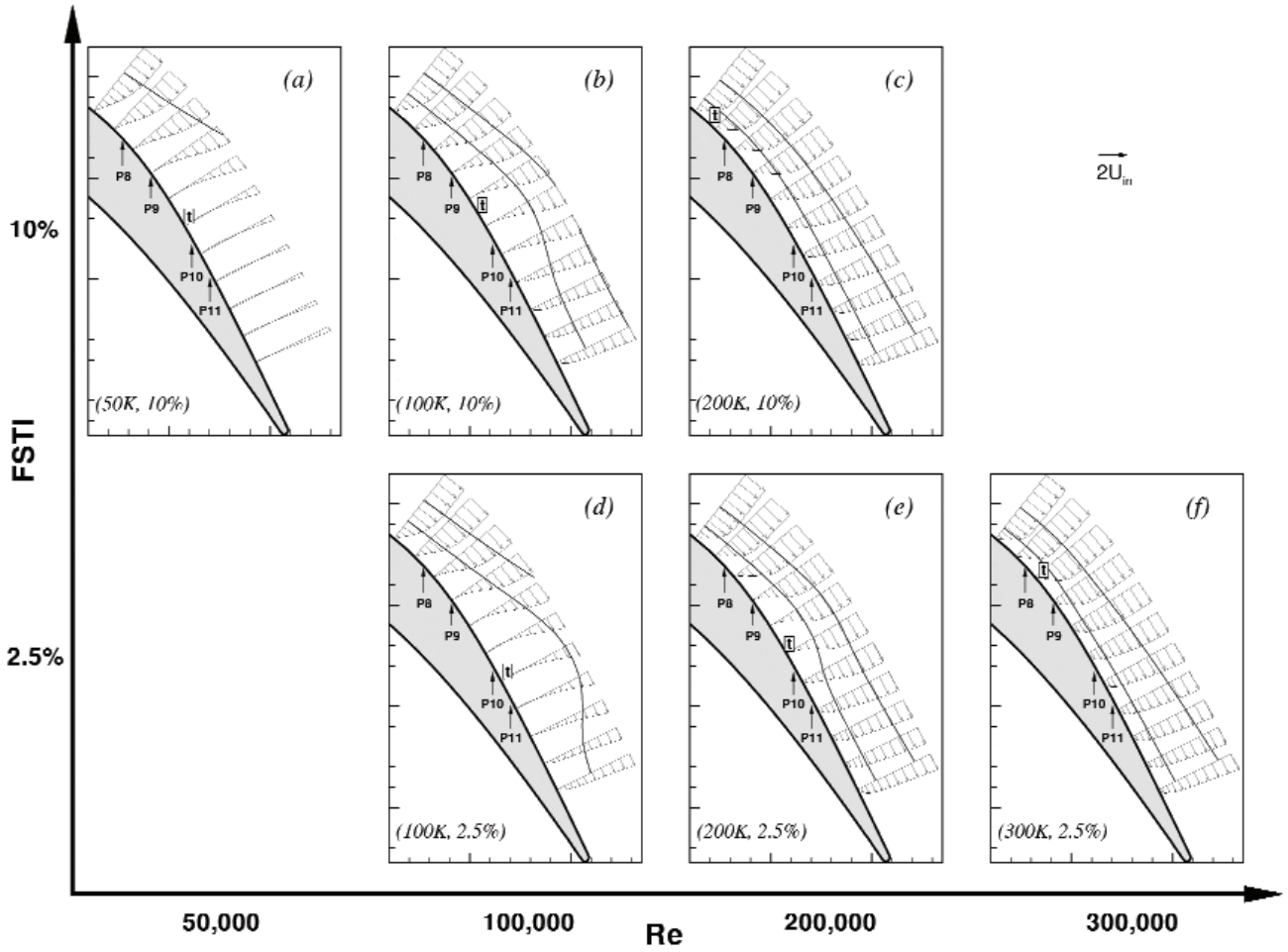


Figure 4. Overall view of a low-pressure turbine flow subject to effects of Reynolds number and freestream turbulence intensity.

processors are used during the computations, it is more efficient to divide the computational domain into several smaller pieces with very fine grids and distribute the zones to processors with the consideration of load balancing. This code has been used extensively in a recent turbulence model validation effort (Hsu *et al*[36]) and simulations of a wide range of low pressure turbine flows (Suzen and Huang[25], Suzen *et al*[30]) conducted at University of Kentucky. All calculations shown in this work employed Menter's two-equation SST turbulence model[31] for computation of turbulent quantities. The final grid systems used for the simulations have been obtained by conducting grid refinement studies in order to ensure that the results presented are grid independent solutions (Suzen and Huang[24], Suzen *et al*[28], Suzen *et al*[29]). In all simulations the grid systems used have first y^+ less then 0·5 near solid walls.

3.0 SIMULATIONS OF LOW-PRESSURE TURBINE BENCHMARK EXPERIMENTS

In the development and validation of the intermittency transport model several low-pressure turbine benchmark test cases ranging from flat plate experiments to unsteady wake–blade interaction experiments were considered. These benchmark experiments representing a wide range of low-pressure turbine operating conditions were chosen to test and validate the predicting capabilities of the intermittency model under diverse flow conditions including the effects of pressure gradients, turbulence intensities, Reynolds number variations, flow separation and reattachment, and unsteady wake–blade interactions.

The following experiments have been used in model development and validation:

- ERCOFTAC benchmarks, Savill[13,14]
- low-pressure turbine experiments of Simon *et al*[15]
- separated and transitional boundary-layer experiments of Volino and Hultgren[16]
- PAK-B blade cascade experiments of Lake *et al*[3,17]
- PAK-B blade cascade experiments of Huang *et al*[18]
- PAK-B blade experiments of Volino[19]
- Unsteady wake–blade interaction experiments of Kaszeta *et al*[20,21]
- Unsteady wake–blade interaction experiments of Stieger[22]

The details and results from simulations of these experiments are described in the next sections.

3.1 ERCOFTAC benchmarks, Savill[13,14]

Initial development and validation of the intermittency model was accomplished using the ERCOFTAC transitional flow benchmark cases assembled by Savill[13,14]. These experiments were specifically designed to test the ability of turbulence models to predict the effects

https://doi.org/10.1017/S0001924000000610 Published online by Cambridge University Press

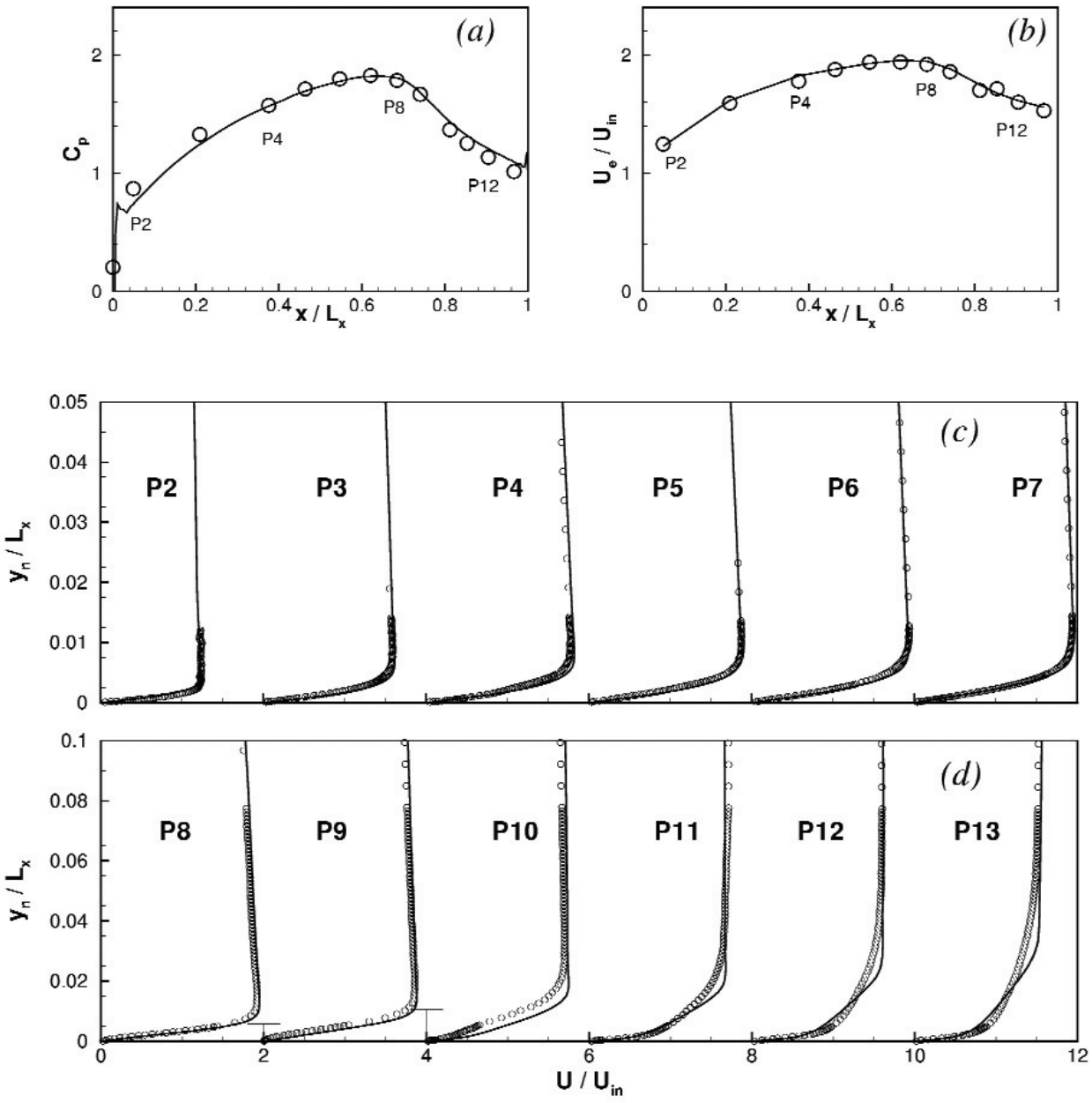


Figure 5. Prediction of the low pressure turbine experiment of Simon *et al*[15], Re = 200,000, FSTI = 10%.

of freestream turbulence on the development and subsequent transition of a laminar boundary layer under zero and varying pressure gradient conditions. Figure 1 shows the skin friction coefficient comparison of the computations using the intermittency transport equation coupled with Menter's SST turbulence model (ITE + Menter SST) against experimental data along with predictions of pure turbulence models for T3A case. T3A is a zero pressure gradient case with freestream turbulence intensity of 3·35% at the leading edge of the plate.

Figure 2 shows comparisons for T3C2 case, which is a variable pressure gradient case with freestream turbulence intensity of 2·8%. For both cases the agreement with the experimental data is very good. The comparisons shown in Figs 1 and 2 illustrate the predicting capabilities of the intermittency transport model under effects of freestream turbulence intensities, zero and variable pressure gradients. The details of model development and validation using ERCOFTAC benchmarks including comparisons with algebraic intermittency models are given in Suzen and Huang[12,23,24].

3.2 Low-pressure turbine experiments of Simon *et al*[15]

Next, the intermittency model is applied to predict the low pressure turbine experiments of Simon *et al*[15] under a wide range of flow conditions. These experiments were conducted to investigate the effect of freestream turbulence intensity and Reynolds number on flow separation and transition in low-pressure turbines.

The test section includes a single PAK-B blade passage. Experiments were conducted for a wide range of Reynolds numbers

https://doi.org/10.1017/S0001924000000610 Published online by Cambridge University Press

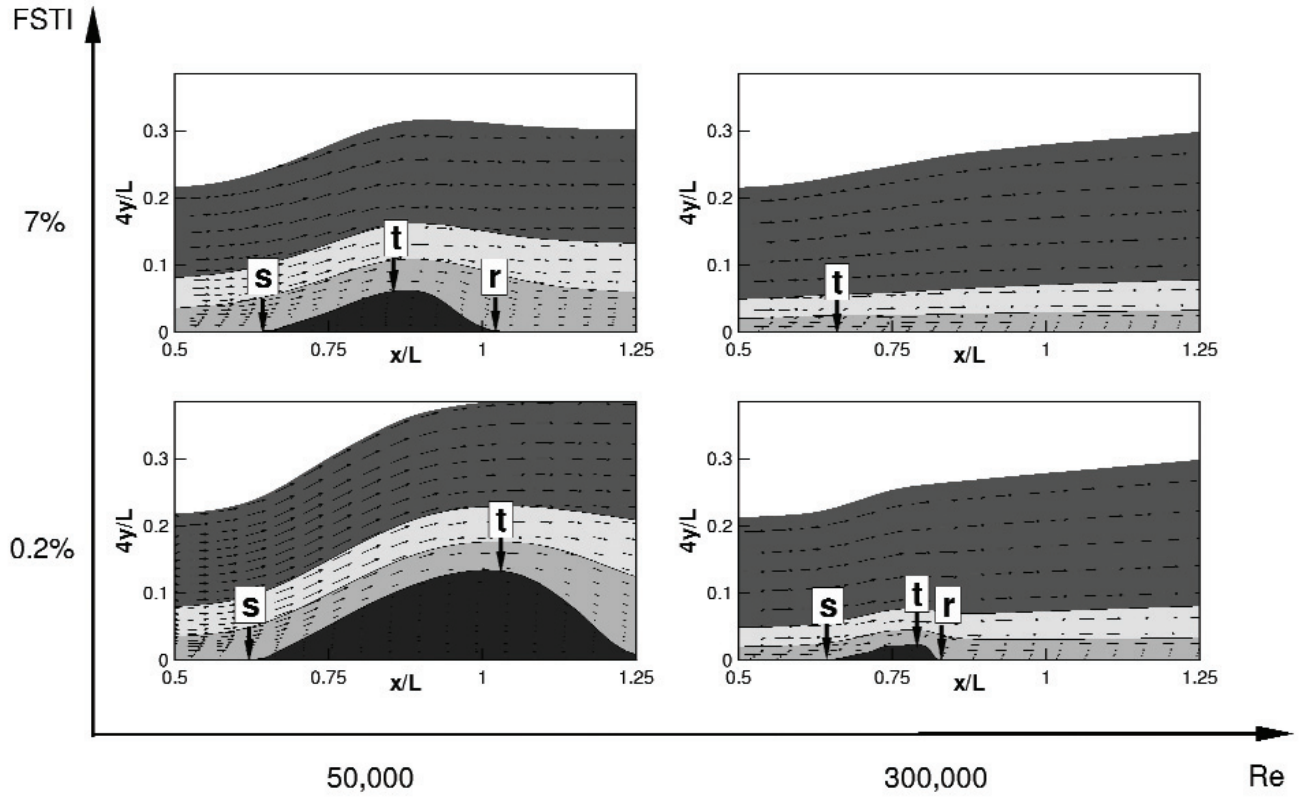


Figure 6. Overall view of effects of Reynolds number and freestream turbulence intensity changes for experiments of Volino and Hultgren[16].

and freestream turbulence intensities. For computations, two freestream turbulence intensity values were considered: one with FSTI = 10% and the other with FSTI = 2·5%. For the cases with FSTI = 10%, three Reynolds numbers were chosen, Re = 50,000, 100,000, and 200,000 and for the FSTI = 2.5% cases, Reynolds numbers selected were, Re = 100,000, 200,000, and 300,000. These cases were selected to test the model's ability in capturing the desired behaviour of flow pattern variations caused by the changes in flow conditions.

Figure 3 shows the comparison of velocity profiles for all measured stations obtained by the current transition model with two other 'pure' turbulence model predictions -one with the Launder-Sharma κ-ε model[37] and the other with the SST model. The experimental flow with Re = 100,000 and FSTI = 10% has been chosen for comparison. Computations using SST model predicted too early transition to turbulence and as a consequence predicted no flow separation. On the other hand, although the κ-ε model predicted the upstream development of the flow very well, the velocity profiles in the downstream portion were poorly represented. Overall, the current transition model showed the best performance throughout the aerofoil suction surface.

Figure 4 shows velocity vectors and streamlines against changes of FSTI and Reynolds number predicted by the intermittency approach. Note that these plots were magnified by a factor of eight in the cross-stream direction. The predicted onset position of transition for each flow was denoted by **t** in the insets of Fig. 4.

For the low Reynolds number case (Re = 50,000 and FSTI = 10%), the flow exhibits a remarkable separation region that begins in a location between the P8 and P9 stations and extends to the P12 station (Figure 4a), and transition occurs between the P9 and P10 positions in the separation bubble. By keeping FSTI the same while increasing Re to 100,000, it is observed that the transition onset moves upstream (still between the P9 and P10 positions), and the separation bubble is suppressed (Fig. 4(b)). If Re is increased to 200,000 while keeping the same FSTI, the prediction shows that the transition onset moves even further upstream (before the P8 position), and the separation bubble disappears, whereas the experiment shows a tiny and thin separation (Fig. 4(c)). On the other hand, if Reynolds number Re is kept at 200,000 while dropping FSTI from 10 to 2·5%, the transition onset moves downstream close to the P10 position, and separation bubble re-appears (Fig. 4(e)). By keeping the same value of FSTI while increasing Reynolds number from 200,000 to 300,000 the transition onset moves upstream again to approximately the P8 position and the separation bubble again disappears (Fig. 4(f)). On the other hand, if Reynolds number is decreased from 200,000 to 100,000, the transition onset point moves downstream to a location between stations P10 and P11 and the separation bubble becomes larger (Fig. 4(d)).

Figure 5 shows comparisons of computed pressure coefficient distribution, freestream velocity distribution, and velocity profiles at 12 stations along the suction surface against experimental data for Re = 200,000 and freestream turbulence intensity (FSTI) of 10%. In this case, the onset of transition was located just before the P8 station, which is the farthest upstream position for all of the cases. As can be seen from the comparison of the pressure coefficient distribution shown in Fig. 5(a), there is no apparent pressure plateau. Fig. 5(b) shows that the predicted variation of the freestream velocity is in excellent agreement with the data. The velocity profiles on the suction surface are predicted reasonably well, as can be seen from Figs 5(c) and 5(d).

The computations using intermittency transport model captured the complex interactions between flow separation and transition observed in the experiments. The good agreement between the computations and the experiments demonstrates the capability of the

https://doi.org/10.1017/S0001924000000610 Published online by Cambridge University Press

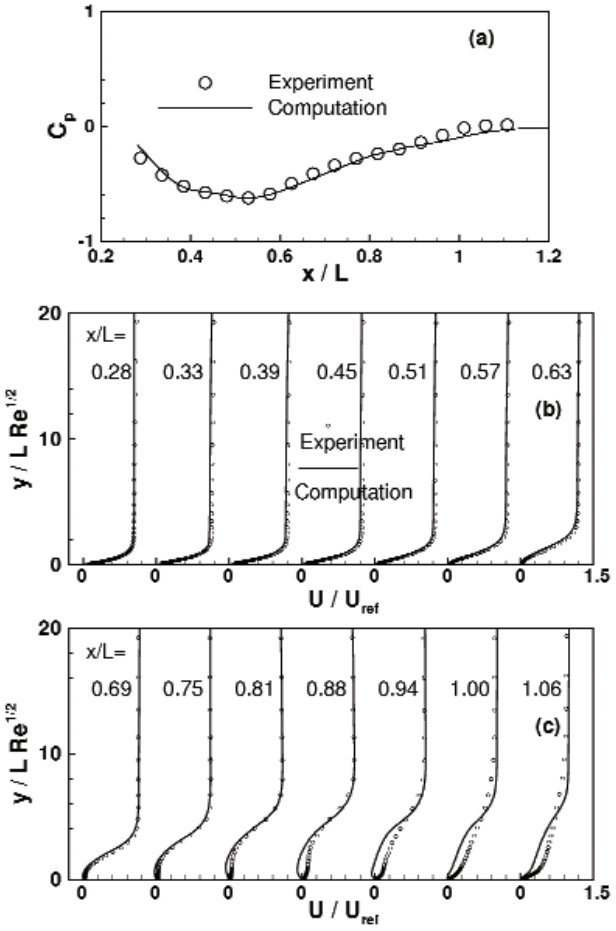


Figure 7. Prediction of experiments of Volino and Hultgren[16], Re = 50,000, FSTI = 7%.

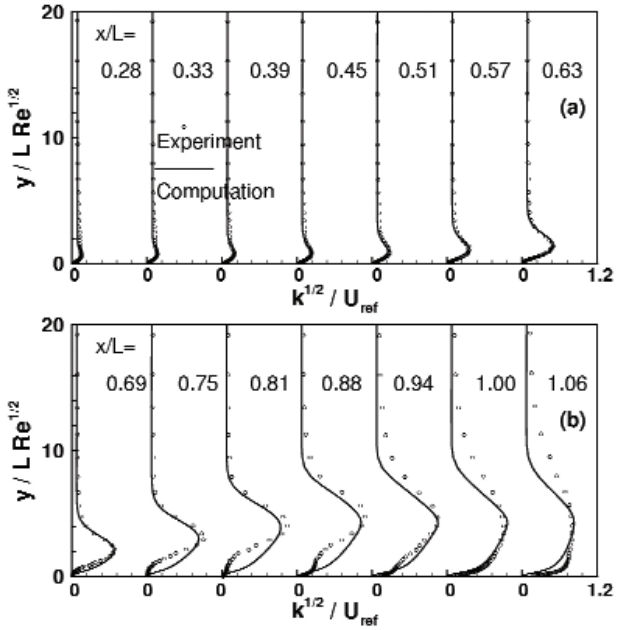


Figure 8. Comparison of turbulence intensity profiles along the surface for experiment of Volino and Hultgren[16], Re = 50,000, FSTI = 7%.

intermittency model in predicting transitional flows in the low-pressure turbine over a range of Reynolds number and FSTI flow conditions. Further detailed results and comparisons for the experiments of Simon *et al*[15] are given in Suzen *et al*[26,28].

3.3 Separated and transitional boundary-layer experiments Volino and Hultgren[16]

Next set of experiments considered for testing and validation of the transition model are the experiments of Volino and Hultgren[16]. These experiments investigated the effects of freestream turbulence and Reynolds number on separated and transitional boundary layers under low-pressure turbine aerofoil conditions. In the experiments, a flat plate boundary layer subject to a streamwise pressure gradient was studied. The superimposed pressure gradients were produced by attaching a two-dimensional contoured shape to the wall opposite to the test surface and by applying suction on the contoured wall. The resultant pressure profile represents that on the suction side of the Pak-B aerofoil. The experiments covered a range of flow conditions including Reynolds numbers between 50,000 and 300,000 and freestream turbulence intensities between 0·2% and 7%. These cases cover a realistic range of operating conditions from takeoff to cruise. On the test wall, velocity, turbulent kinetic energy and intermittency profiles were measured at fourteen streamwise stations. In the measurements, quantities such as skin friction coefficients, transition start and end locations, and the locations of separation and reattachment were also determined. Further details of the measurements and experimental data are given by Volino and Hultgren[16]. These experiments provide a good set of data for the development and validation of models for flow transition.

The experiment considered in this study involves two different Reynolds numbers, Re = 300,000 and Re = 50,000 (based on nominal exit velocity and wetted plate length) and two freestream turbulence intensities, FSTI = 7% and FSTI = 0·2%. Figure 6 depicts the dynamic interplay between transition and separation when subject to variations in Reynolds number and freestream turbulence effects. In this figure the insets **s** and **t** denote the onset of separation and transition, respectively and the inset **r** denotes the reattachment point. The first case considered is with Re = 300,000 and FSTI = 7%. For this case, the transition position is at x/L=0·66 and only a tiny flow separation is observed near x/L = 0·7. As the Reynolds number is decreased from 300,000 to 50,000 while keeping the freestream turbulence intensity the same, the onset of transition is delayed until x/L = 0·85. As a result of the delay of the transition, a sizable flow separation is encountered between x/L = 0·7 and x/L = 1·0.

On the other hand, when the turbulence intensity is decreased from 7% to 0·2% while the Reynolds number is maintained at 300,000, the transition onset is delayed until x/L = 0·79. As a result, a small but visible separation bubble is observed in the vicinity of x/L = 0·75. The last case involved a simultaneous decrease of Reynolds number and freestream turbulence intensity, from 300,000 to 50,000 and from 7% to 0·2%, respectively. In this case the onset of transition is delayed to x/L = 1·03 and a massive separation extending from x/L = 0·7 to x/L = 1·25 is observed. The current prediction accurately captured the above-mentioned dynamic behaviour of the interaction between transition and separation when subject to changes in Reynolds number and freestream turbulence intensity conditions.

In order to illustrate the predicting capabilities of the intermittency model, comparisons of computed results and experiment for Re = 50,000, FSTI = 7% are shown in Figs 7 and 8. The pressure coefficient distribution is compared to experiment in Fig. 7(a). The agreement with the experiment is good except in the region after x/L = 0·95, where it can be seen that the pressure coefficient is slightly under predicted indicating that the streamwise velocity distribution

https://doi.org/10.1017/S0001924000000610 Published online by Cambridge University Press

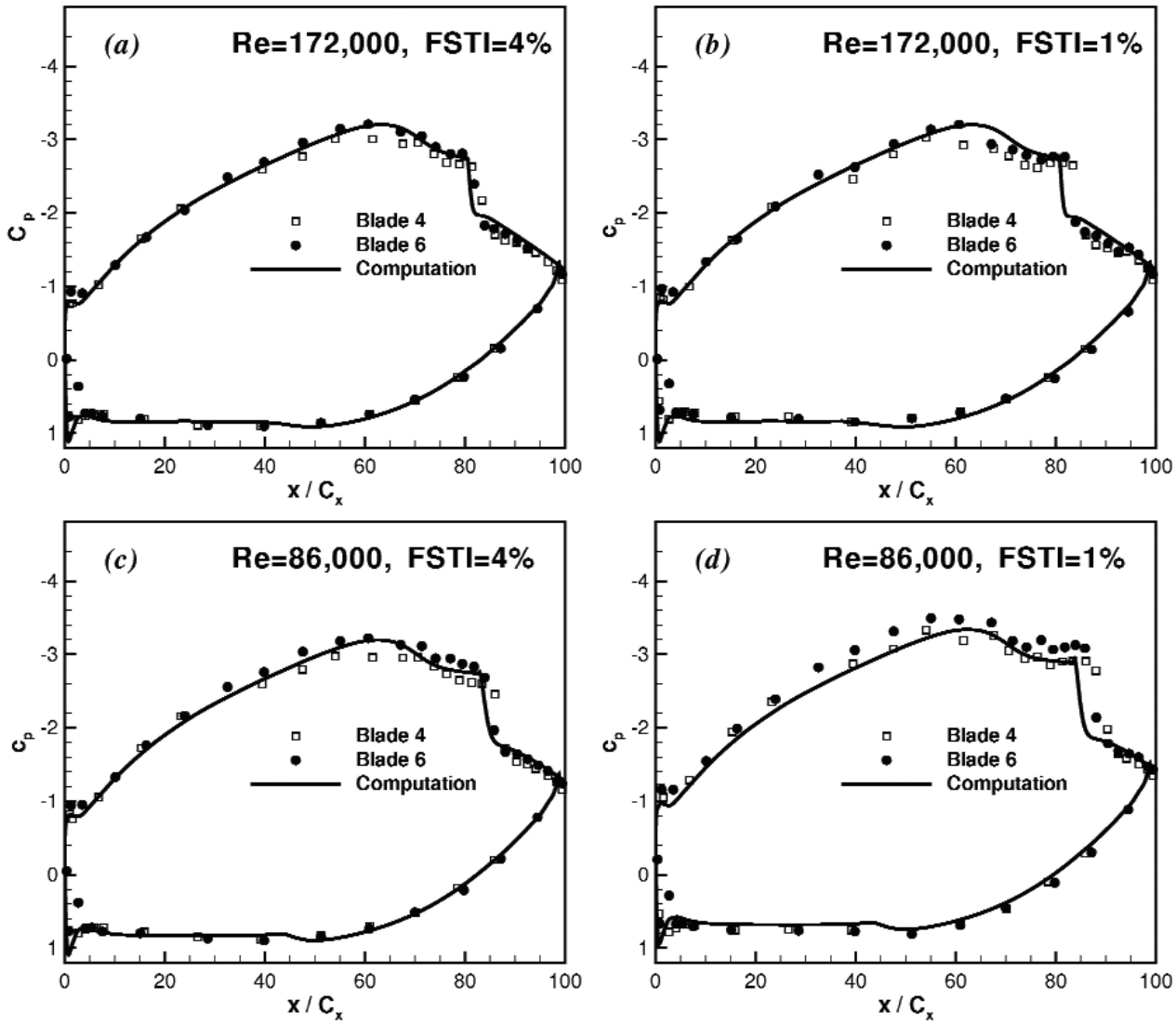


Figure 9. Comparison of computed pressure coefficient distributions with experiments of Lake *et al*[3,17].

is slightly over predicted. The comparisons of velocity profiles are given in Figs 7(b) and 7(c). The profiles are in good agreement with the experiment up to x/L = 0·88. The experimental data shows that the flow attaches after x/L = 0·94 whereas the predictions indicate that the separation is extended up to x/L = 1·0. In Figs 8(a) and 8(b), comparisons of turbulence intensity profiles are shown. It can be seen that the comparisons between predictions and experimental data are favorable.

These computations demonstrate the versatility of the transition model for flows under diverse conditions. Detailed results and comparisons for the experiments of Volino and Hultgren[16] including intermittency profiles are given in Suzen *et al*[27,29].

3.4 PAK-B blade cascade experiments of Lake *et al*[3,17]

Lake *et al*[3,17] conducted experiments on the PAK-B blade in order to identify methods for reducing separation losses on low-pressure turbine blades under low Reynolds number conditions. In the experiments, they investigated flows at low Reynolds numbers of 43,000, 86,000, and 172,000 based on inlet velocity and axial chord and freestream turbulence intensities of 1% and 4%. These conditions are similar to those encountered at high altitude, low speed flight of reconnaissance unmanned aerial vehicles used by USAF. Measurements were made on unmodified (baseline) and modified PAK-B blade. For the unmodified blade, surface pressure coefficients, boundary-layer velocity and turbulence profiles, total pressure loss data were obtained.

The intermittency model is applied to predict the PAK-B blade experiments of Lake *et al*[3,17]. In the computations flows at Reynolds numbers of 86,000, and 172,000 based on inlet velocity and axial chord with freestream intensities of 1% and 4% were investigated. The Reynolds numbers correspond to 205,000 and 409,000 based on the exit velocity and suction surface length.

The first cases considered correspond to Re = 172,000 with two freestream turbulence intensities. The computed pressure coefficient distributions are compared to experiment for freestream turbulence intensities of 4% and 1% in Figs 9(a) and 9(b), respectively. In the figures, the experimental distributions correspond to the measurements

https://doi.org/10.1017/S0001924000000610 Published online by Cambridge University Press

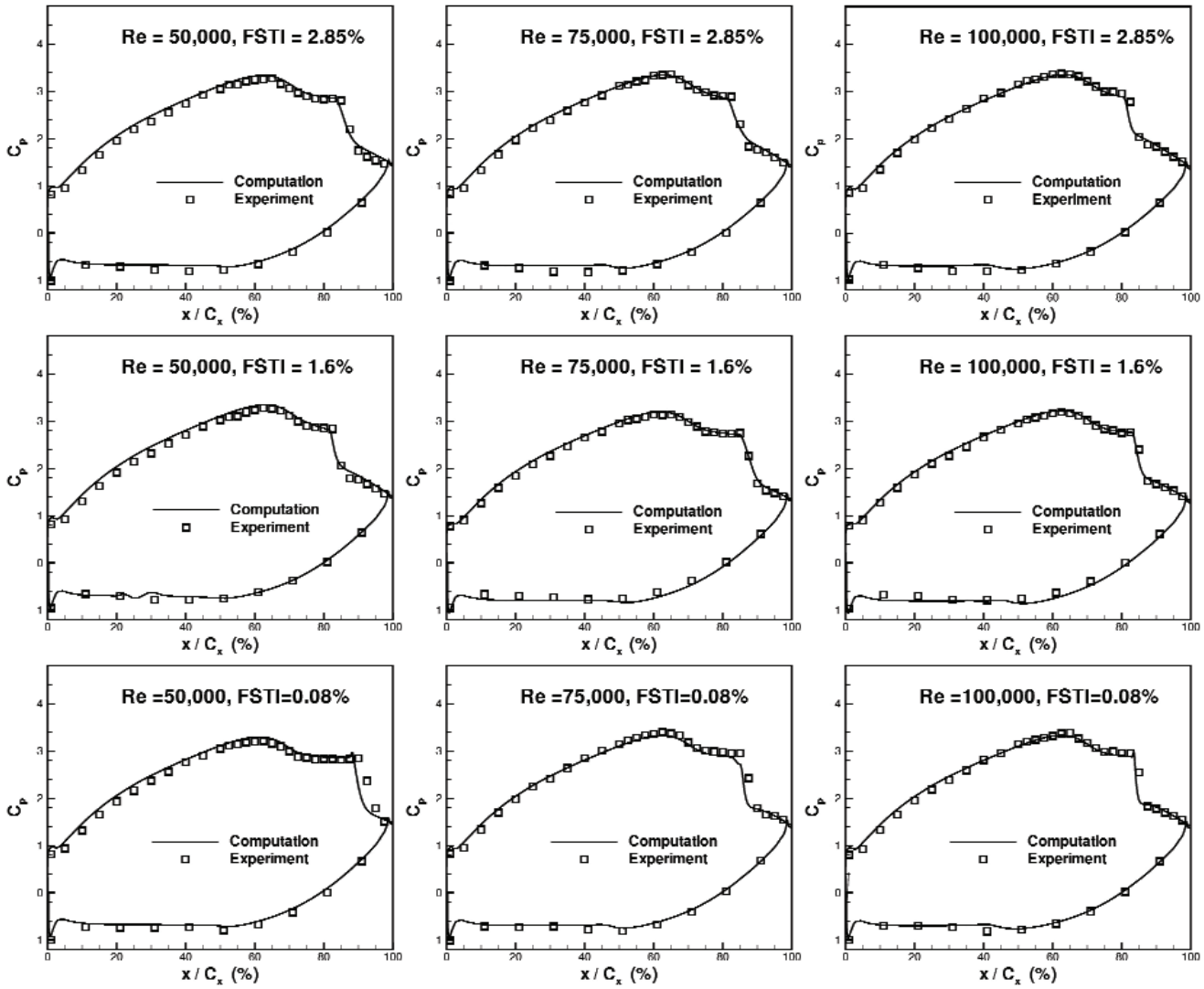


Figure 10. Comparison of computed pressure coefficients with experiments of Huang *et al*[18].

made on test blades 4 and 6. For the high turbulence intensity, FSTI = 4%, flow separation is observed on the suction surface at $x/L_x = 0{\cdot}73$ in computations compared to the experimental location of $x/L_x = 0{\cdot}78$ and the onset of transition is at $x/L_x = 0{\cdot}8$ in the computations. The computed pressure coefficient distribution compares well with the experimental data as shown in Fig. 9(a). For FSTI=1%, the flow separates on the suction surface at $x/L_x = 0{\cdot}72$ and the onset of transition is computed to be at $x/L_x = 0{\cdot}8$. In the experiment flow separation takes place at $x/L_x = 0{\cdot}75$ and the extent of separation bubble is larger than the one observed in the computation. This is evident in Fig. 9(b) from the pressure plateau between $x/L_x = 0{\cdot}73$ and $x/L_x = 0{\cdot}83$ in the experimental C_p distribution. The onset of transition location is not available from the experiments.

Next, Reynolds number is reduced to 86,000 and the computed pressure coefficient distributions for FSTI = 4% and FSTI = 1% are compared to experiment in Figs 9(c) and 9(d), respectively. For both cases the onset of transition on the suction surface is approximately at $x/L_x = 0{\cdot}85$. For FSTI = 4% the flow separation is at $x/L_x = 0{\cdot}74$ from computation and at $x/L_x = 0{\cdot}77$ in the experiment. The C_p distribution compares well with the experiment as shown in Fig. 9(c). The flow separation is predicted at $x/L_x = 0{\cdot}72$ for FSTI = 1% compared to $x/L_x = 0{\cdot}73$ of experiment. In the computation the flow reattaches earlier than it does in the experiment as can be observed in Fig. 9(d) from the difference in the pressure coefficient distributions between $x/L_x = 0{\cdot}8$ to $0{\cdot}85$. Overall, computations compare well with the experiments. Detailed comparisons of computations with experiments of Lake *et al*[3,17] are given in Suzen *et al*[30].

3.5 PAK-B blade cascade experiments of Huang *et al*[18]

Huang *et al*[18] conducted experiments on PAK-B blade cascade for a range of Reynolds numbers and turbulence intensities. The Reynolds numbers range from 10,000 to 100,000 based on inlet velocity and axial chord which correspond to 11,036 to 110,360 based on inlet velocity and chord length. The freestream turbulence intensity levels considered in the experiments were 0·08%, 1·6%, and 2·85%. In the computations, experiments performed for Reynolds numbers 50,000, 75,000, and 100,000 were considered. Pressure coefficient data is available for all cases and detailed boundary-layer measurements are available for Re = 50,000, 75,000, and 100,000 with FSTI = 0·08% and 2·85% cases.

The computed pressure coefficient distributions are compared to experimental data in Fig. 10. The computations with the transition

https://doi.org/10.1017/S0001924000000610 Published online by Cambridge University Press

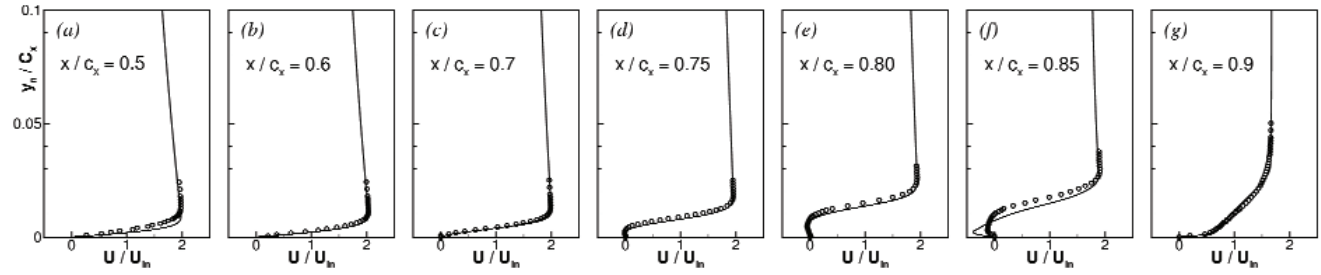


Figure 11. Comparison of computed velocity profiles with experiment for experiments of Huang *et al*[18], Re = 75,000, FSTI = 0·08%.

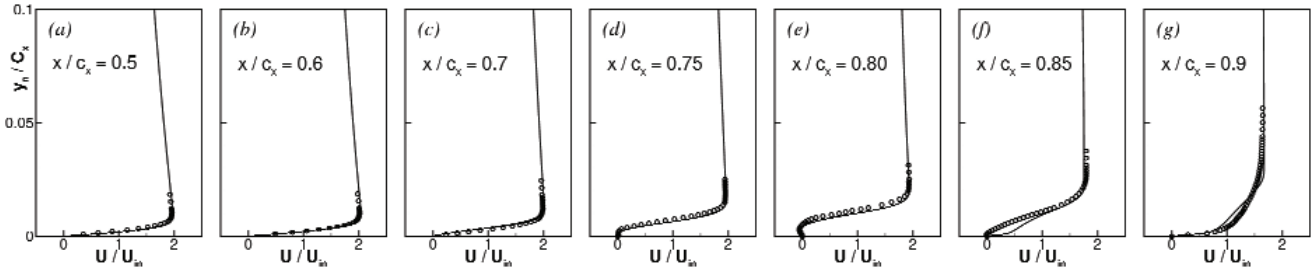


Figure 12. Comparison of computed velocity profiles with experiment for experiments of Huang *et al*[18], Re = 75,000, FSTI = 2·85%.

model compare well with the experimental data for all cases considered. In this figure the comparisons are organised such that the vertical axis denotes the freestream turbulence intensity whereas the horizontal axis corresponds to Reynolds number. At a given FSTI, for example 2·85%, as Reynolds number is increased from 50,000 to 100,000, the extent of the separation bubble on the suction surface of the blade characterised by the plateau in the pressure coefficient distribution gets smaller as can be observed from Fig. 10. Also, at a chosen Reynolds number, for example Re = 75,000, if the FSTI is increased from 0·08% to 2·85% the same trend in separation bubble size is observed. The change in separation bubble size can be clearly seen in the velocity profile comparisons shown in Figs 11 and 12 for Re = 75,000, FSTI = 0·08%, and FSTI = 2·85%, respectively. The separation bubble for FSTI = 0·08 cases is much longer and thicker when compared to the FSTI = 2·85% case. The computed velocity profiles compare well with the experimental data illustrating the ability of the model to capture the effects of Reynolds number variations, FSTI, and flow separation on transition. Further detailed comparisons of computations with experiments of Huang *et al*[18] are given in Suzen *et al*[30].

3.6 PAK-B blade experiments of Volino[19]

Volino[19] investigated the boundary-layer separation, transition, and reattachment under low-pressure turbine aerofoil conditions. The experiments included five different Reynolds numbers in terms of inlet velocity and chord length ranging between 10,291 to 123,492 and freestream turbulence intensities of 0·5% and 9%. The test section consisted of a single passage between two PAK-B blades. The compiled data include pressure surveys, mean and fluctuating velocity profiles, intermittency profiles, and turbulent shear stress profiles. These experimental results provide detailed documentation of the boundary layer and extend the existing database to lower Reynolds numbers.

Computed pressure coefficient distributions are compared to experiments in Figs 13(a) through 13(d) for Re = 82,324, 41,162, 20,581, and 10,291 with FSTI = 0.5%. Computed velocity profiles are compared to experiment at 11 stations along the suction surface of the blade in Figs 14 through 17 for these Reynolds numbers. Overall, the computed velocity profiles and pressure coefficients compare well with the experimental data. Details of the experiments of Volino[19] and further comparisons of predictions with experiments are given in Suzen *et al*[30].

3.7 Unsteady wake–blade interaction experiments of Kaszeta *et al*[20,21]

In order to investigate the effects of periodically passing wakes on laminar-to-turbulent transition and separation in a low-pressure turbine passage, Kaszeta *et al*[20,21] conducted a number of experiments. The test section was designed to simulate unsteady wakes in turbine engines for studying their effects on boundary layers and separated flow regions over the suction surface. The turbine blade passage simulator used in the experiment was a modified version of the simulator used by Qui and Simon[38] and Simon *et al*[15] consisting of a single suction surface and a single pressure surface to simulate a single PAK-B turbine blade passage. In order to produce the periodic wakes upstream of the turbine blade leading edge a wake generator was added. The wake generator consisted of a moving sled assembly which contained a series of 0·635cm steel rods to simulate wakes emerging from upstream turbine stages in a LPT. A cross-sectional view of the experimental facility is shown in Fig. 18. The spacing between rods and between blade surfaces is 80% of the blade chord length. The rods are located 12 rod diameters upstream from the leading edges.

In the experiment, the Reynolds number based on the suction surface length and exit velocity is 50,000 (~22,875 based on inlet velocity and chord length) and the freestream turbulence intensity is 2·5%. The initial set up has the rod spacing equal to the blade pitch (L_r/P = 1). In order to examine the effects of reduced wake frequency, additional experiments were performed increasing the rod spacing to twice the blade pitch (L_r/P = 2) while keeping everything else the same. In addition, effects of elevated approach flow turbulence intensity are also investigated[20,21,39-41].

https://doi.org/10.1017/S0001924000000610 Published online by Cambridge University Press

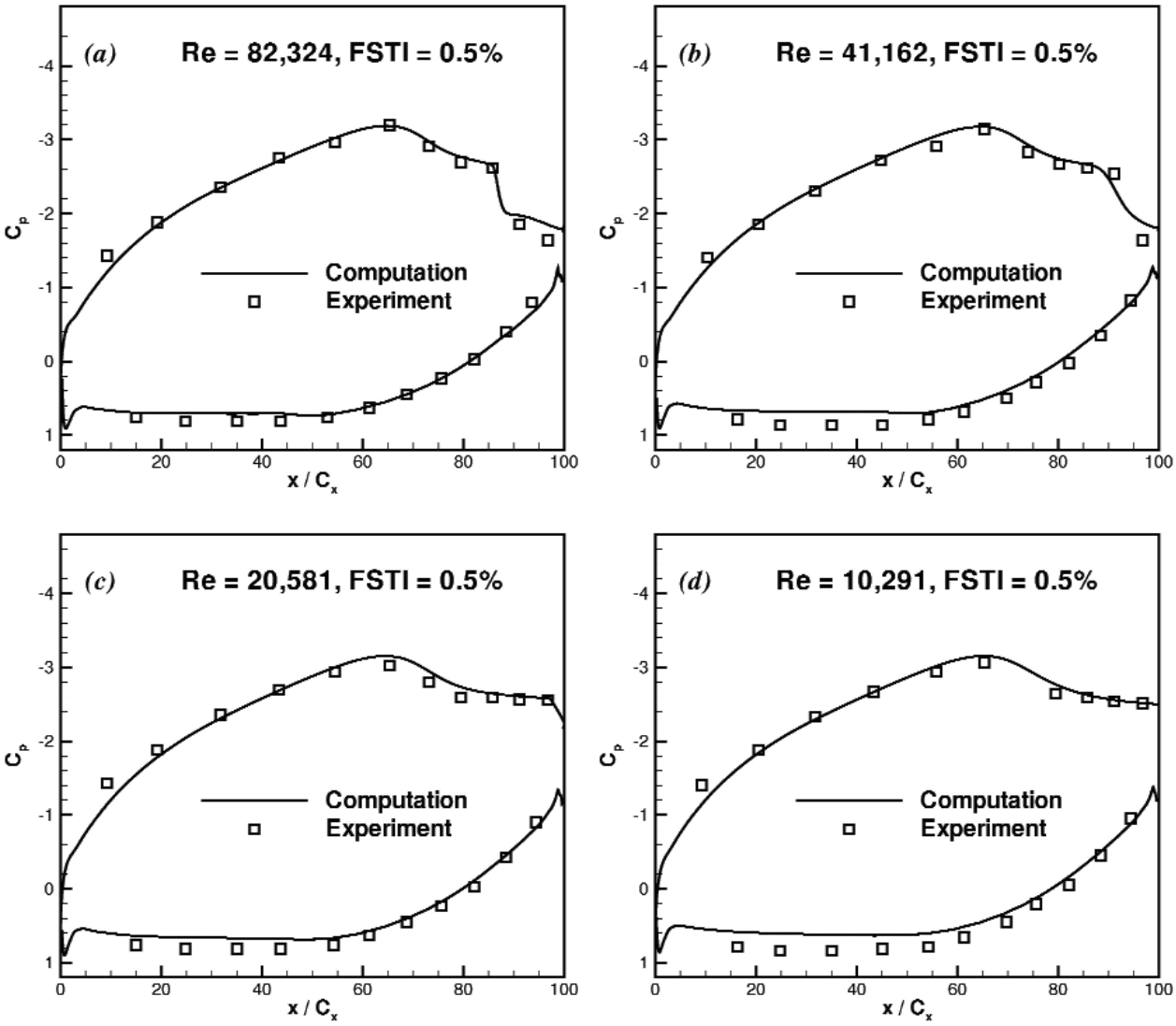


Figure 13. Comparison of computed pressure coefficient with experiments of Volino[19].

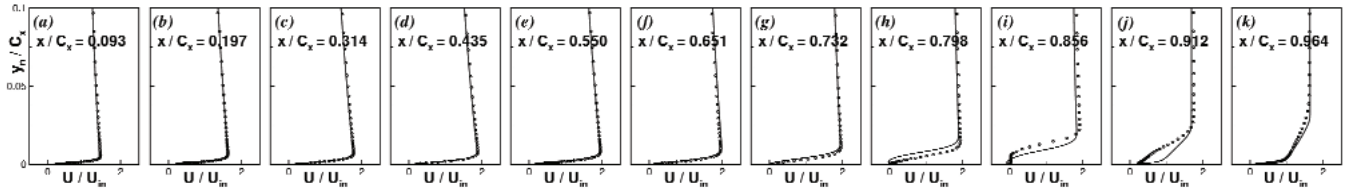


Figure 14. Comparison of computed velocity profiles with experiment for experiments of Volino[19], Re = 82,324, FSTI = 0·5%.

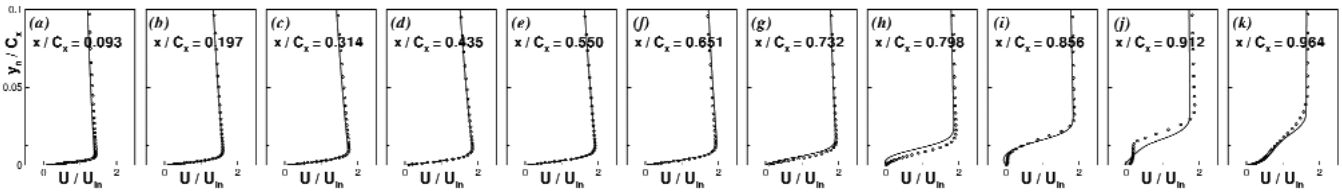


Figure 15. Comparison of computed velocity profiles with experiment for experiments of Volino[19], Re = 41,162, FSTI = 0·5%.

https://doi.org/10.1017/S0001924000000610 Published online by Cambridge University Press

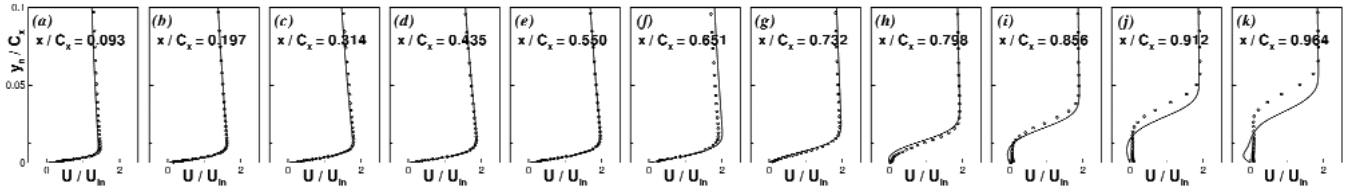


Figure 16. Comparison of computed velocity profiles with experiment for experiments of Volino[19]), Re = 20,581, FSTI = 0·5%.

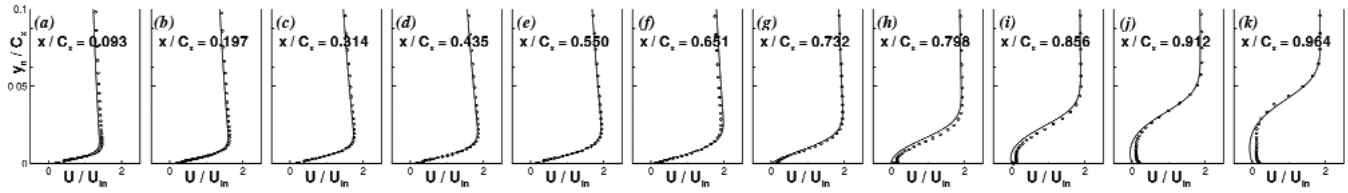


Figure 17. Comparison of computed velocity profiles with experiment for experiments of Volino[19]), Re = 10,291, FSTI = 0·5%.

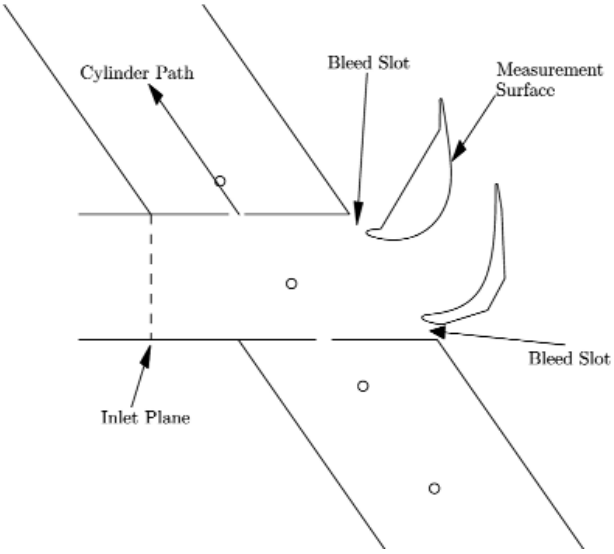


Figure 18. Cross-sectional view of the wake generator passage, Kaszeta *et al*[20]).

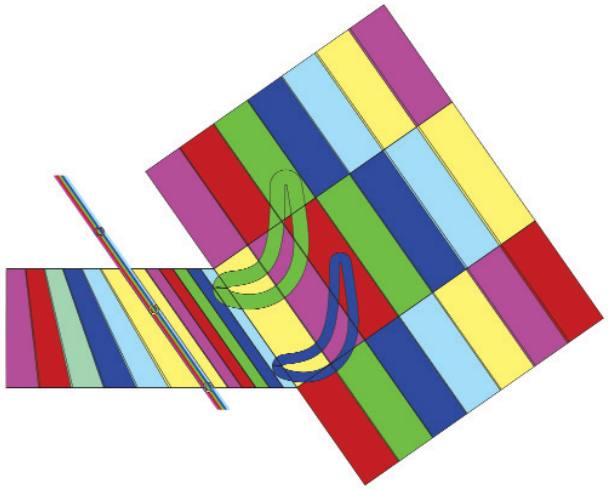


Figure 19. Multi-block grid system used for simulating experiment of Kaszeta *et al*[20,21]).

The experiment of Kaszeta *et al*[20,21]) is simulated using the forty three zone multi-block grid shown in Fig. 19. Three rod grids are overset in zones extending outside from the bottom and top of the inflow channel. These zones combined with the rod grids slide up with the specified experimental rod speed value of 70% of the axial flow velocity and periodic boundary conditions imposed at top and bottom boundaries in order to simulate continuous succession of rods.

The grid system shown in Fig. 19 corresponds to the experimental set up with the rod spacing equal to the blade pitch referred to as 'high wake frequency case'. In order to simulate the reduced wake frequency case where the rod spacing is twice the blade pitch (referred to as 'reduced wake frequency case'), only one rod grid is employed and the length of the zones extending outside the inflow channel were adjusted to enable employment of periodic boundary conditions at top and bottom boundaries.

The comparisons of the computed and experimental mean velocity profiles for the high and reduced wake passing frequency cases are presented in Figs 20 and 21, respectively. In Fig. 20, the comparison is considered to be fair. The simulations predict a larger separation bubble evident from the velocity profiles at stations P9 through P12.

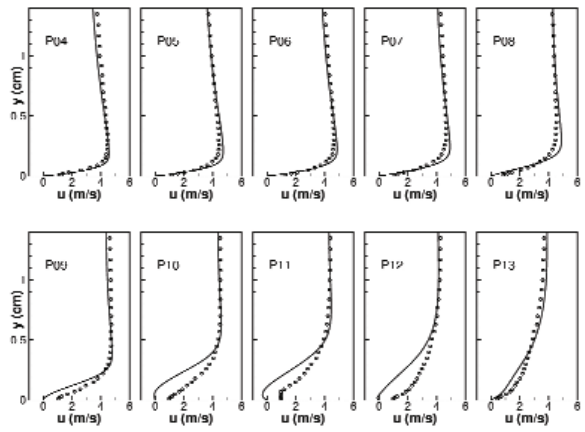


Figure 20. Comparison of mean streamwise velocity profiles at Stations P04 through P13 for high wake passing frequency case of Kaszeta *et al*[20,21]).

https://doi.org/10.1017/S0001924000000610 Published online by Cambridge University Press

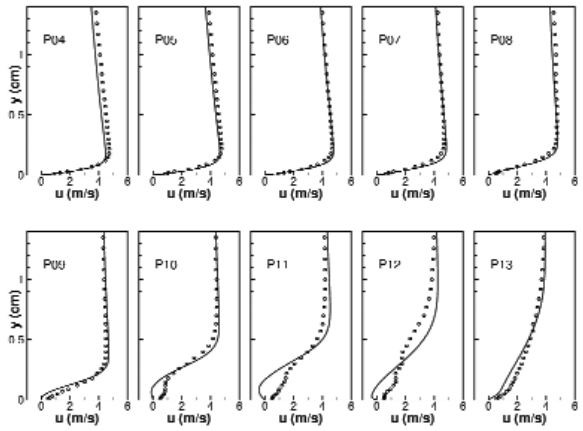


Figure 21. Comparison of mean streamwise velocity profiles at Stations P04 through P13 for reduced wake frequency case of Kaszeta *et al*[20,21].

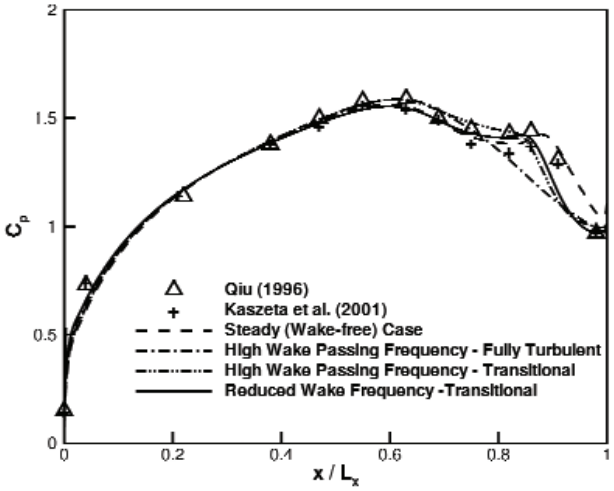


Figure 22. Pressure coefficient comparison for experiment of Kaszeta *et al*[20].

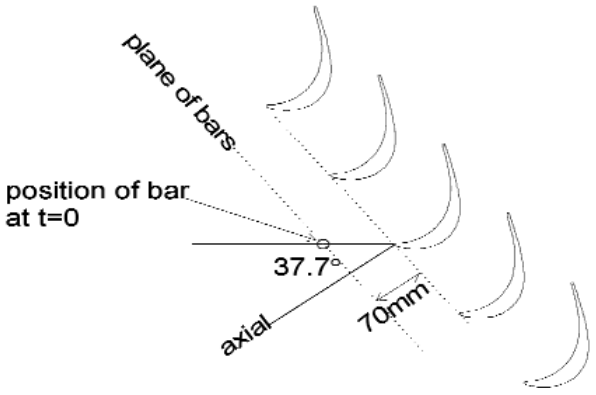


Figure 23. Details of the bar passing cascade from Stieger[22].

Table 1
T106 cascade details from Stieger[22]

Chord	198mm
Blade stagger	59·3°
Cascade pitch	158mm
Inlet flow angle	37.7°
Design exit flow angle	63·2°
Bar diameter	2·05mm
Axial distance: bars to LE	70mm
Flow coefficient (U_{axial}/U_{bar})	0·83

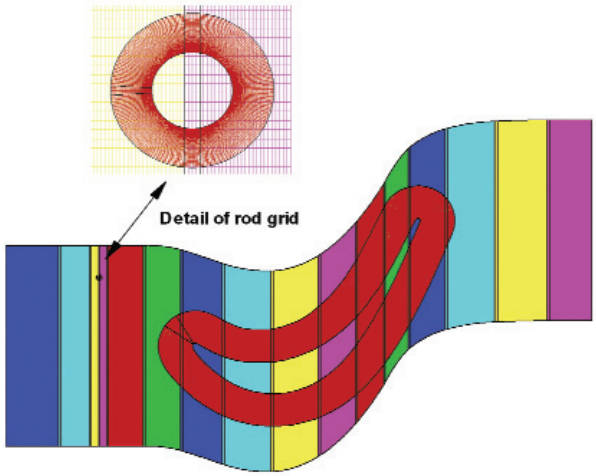


Figure 24. Multi-block grid system used in simulations of experiments of Stieger[22].

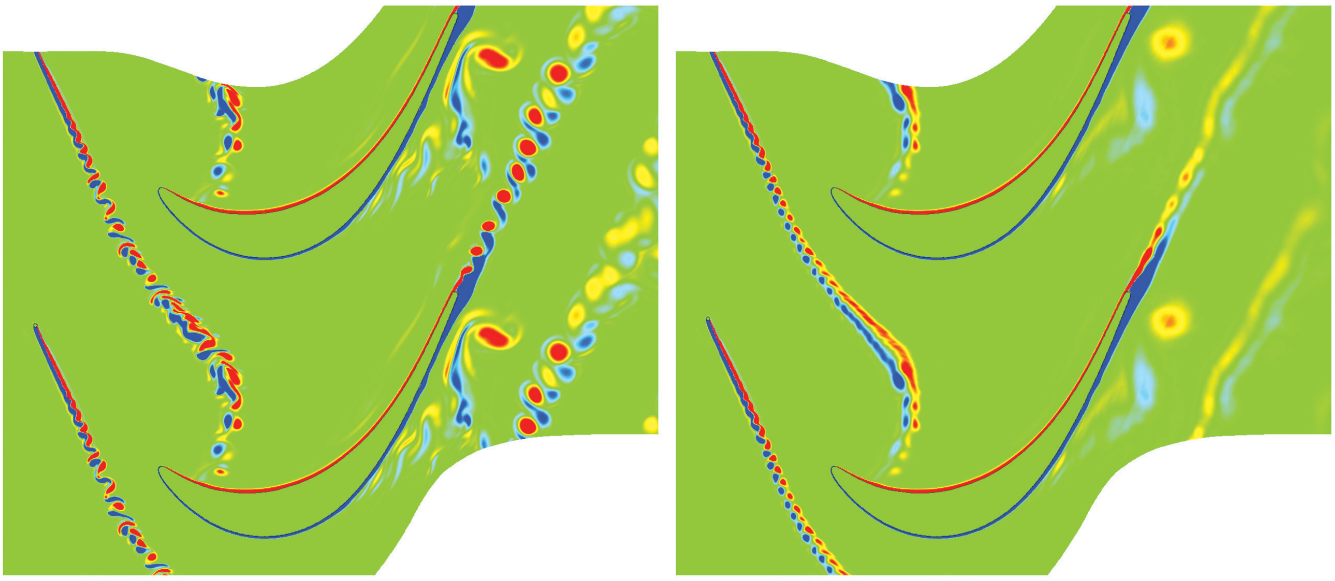
It should be noted that the hot wire is not adequate for velocity measurement when flow separation occurs. The fact that the experimental data do not approach zero, as at stations P9 to P11, indicates that the flow may be separated.

The comparison of mean velocity profiles for the reduced wake passing frequency case shown in Fig. 21 illustrate the good agreement between the simulations and the experiments. It must be noted that the discrepancy between the profiles in the near wall region at stations P10 through P12 in Fig. 21 is due to the inability of the hot wire to measure reversed flows.

The pressure coefficient distribution comparisons are given in Fig. 22. In this figure the experimental data correspond to wake-free steady-state flow. The computed results include fully turbulent and transitional simulations for the high wake passing frequency case, transitional simulations for reduced frequency case and wake-free steady-state case.

The experimental data show a plateau of the pressure distribution after $x/L_x = 0{\cdot}7$ indicating a flow separation while the fully turbulent computation misses it completely. The simulation for the high wake frequency case incorporating the intermittency transport model indicates separated flow in that region, however, the extent of the separation zone is shorter when compared to the wake-free computation and experiment. These results agree with the conclusions drawn from the experiments that the effect of passing wakes is to change the location of separation and reduce the size of the separation bubble due to increase in turbulence levels by wakes when compared to wake-free flow. For the reduced frequency case, separation bubble is larger than the high wake frequency case and closer in size and location to experiment and wake-free computation. It is evident that the effect of reduced wake frequency is to enlarge the separation zone. This is due to the fact that the reduced wake frequency, that is, increased wake temporal spacing, allows the boundary layer on the suction surface of

https://doi.org/10.1017/S0001924000000610 Published online by Cambridge University Press



(a) Instantaneous (b) Phase averaged

Figure 25. Computed vorticity contours for experiment of Stieger[22].

the blade a much longer time to recover from the perturbations of the wakes and allows the boundary layer to reach a state which is much like the steady flow case without the moving bars.

Overall, simulations were able to capture the flow features well for experiments of Kaszeta *et al*[20,21]. The prediction capabilities of the intermittency transport model for simulations of unsteady wake–blade interaction flowfields are illustrated. Further details of these simulations can be found in Suzen and Huang[25].

3.8 Unsteady wake–blade interaction experiments of Stieger[22]

The experiments performed by Stieger[22] involve T106 turbine blade cascade subjected to wake passing from a moving bar wake generator. These experiments were conducted in order to investigate the interaction of a convected wake and a separation bubble on the rear suction surface of a highly loaded low-pressure turbine blade. The wakes shed from upstream blade rows in a real turbine are simulated by an array of cylindrical bars moving across the inlet plane of the cascade.

The unsteady wake-passing flow conditions were chosen to match those of a repeating stage of the T106 profile. The Reynolds number based on chord and inlet velocity was Re = 91,077 and the freestream turbulence intensity was FSTI = 0·1%. The flow coefficient for the cascade was ϕ = 0·83. The bar pitch matched the cascade pitch so that s_b/s_c = 1. The bar diameter of 2·05mm was chosen to match the loss of a representative turbine blade. The cascade incidence was set to α_1 = 37·7°. The details of the T106 cascade set up are shown in Fig. 23 and are summarised in Table 1.

In the experiments, a series of boundary-layer traverses were performed using 2D LDA. The results obtained provided new insight into the wake-induced transition mechanisms on low-pressure turbine blades.

Simulations of experiments of Stieger are performed using the multi-block grid system consisting of 18 zones and 0·8m grid points shown in Fig. 24. The rod grid shown in the inset and the two zones it overlaps move with the specified bar speed of 1·2 times the axial flow velocity. The grid system has the first y^+ less than 0·5 near solid walls. The origin is located at the leading edge of the blade for this grid system. Periodic boundary conditions are employed at top and bottom boundaries.

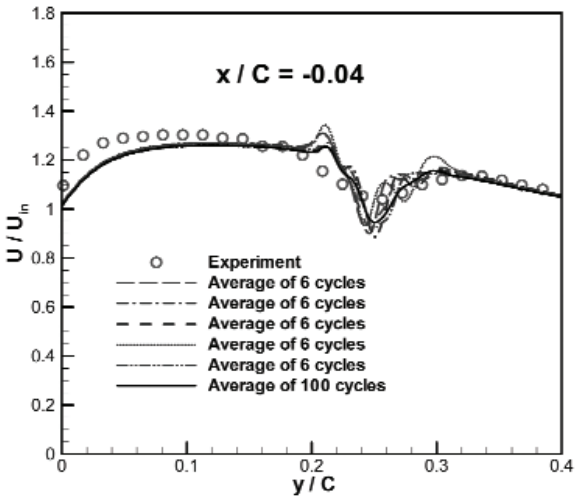


Figure 26. Comparison of computational and experimental wake velocity profiles before the blade leading edge for experiments of Stieger[22].

Predicted instantaneous and phase averaged vorticity isocontours are shown in Figs 25(a) and (b), respectively. In this case the Reynolds number based on bar diameter and flow speed over the bar is 1,650. The instantaneous vortex shedding behind the bar is sharper and the wake is narrower when compared to the phase averaged contours. The smoothing effect of phase averaging is evident from the wake velocity profile shown in Fig. 26.

In Fig. 26, the predicted wake velocity profile is compared to experiment at a location of x/C = –0·04 before the blade leading edge. The phase averages of five different sets of six-cycle data is shown along with the phase average of hundred cycles. The fluctuations are apparent in each of the six-cycle averages. However, these fluctuations are smoothed out as a larger number of cycles are included in averaging. The average of 100 cycles closely represent the wake profile observed in the experiment.

https://doi.org/10.1017/S0001924000000610 Published online by Cambridge University Press

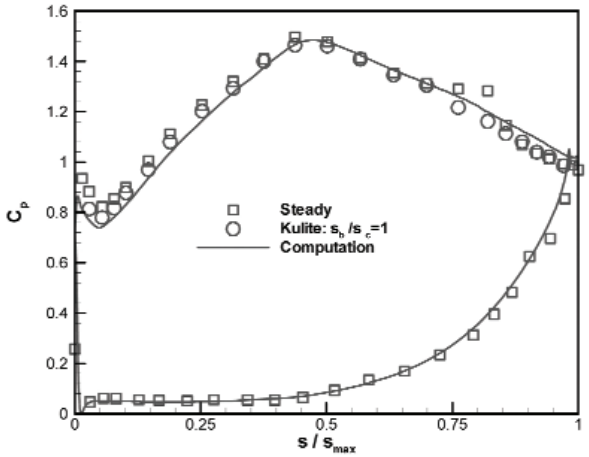


Figure 27. Comparison of computational and experimental pressure coefficient distributions for experiments of Stieger[22].

The predicted time average pressure coefficient distribution compares well with the experiment as shown in Fig. 27. In this figure the steady state experiment without the moving bars is also included in order to illustrate the effect of wake interaction on the suction side pressure distribution. In the steady state case, there is a large separation bubble on the suction side of the blade characterised by the plateau in the pressure coefficient distribution between s/s_o = 0·7 and 0·83. On the other hand, time average C_p distribution obtained from the case with moving bars does not exhibit such a plateau, indicating attached mean flow over the suction surface. This is due to the effect of the wakes interacting with the boundary layer on the suction surface causing transition to turbulence and hence reducing the susceptibility of the flow to separate.

Comparisons between the computed and experimental phase-averaged streamwise velocity variations at nine stations on the suction side of the blade are shown in Figs 28(a) through 28(i). In these figures, the horizontal axis corresponds to the phase angle in degrees and the vertical axis correspond to the distance normal to the wall nondimensionalised by chord. The numerical results are in good agreement with the experiment. The movement of the wake interaction region characterised by the maximum velocity is captured well in the simulations.

The predicted mean velocity profiles at nine stations along the suction surface are compared to experiment in Fig. 29. The simulations agree very well with the experimental data.

The good agreement obtained between the simulations and the experimental data illustrate the predicting capabilities and versatility of the transition model in predicting unsteady wake–blade interaction flowfields.

4.0 CONCLUDING REMARKS

A transport equation for the intermittency factor is employed to predict a wide range of low-pressure turbine experiments representing the effects of diverse flow conditions on transition including the effects of pressure gradients, freestream turbulence intensities, Reynolds number variations, flow separation/reattachment, and unsteady wake–blade interactions. The intermittent behaviour of the transitional flows is taken into account by modifying the eddy viscosity with the intermittency factor. Comparisons of the computed and experimental data are made and overall good agreement with the experimental data is obtained demonstrating the predicting capabilities of the current intermittency approach and the intermittency transport model. Although its dependence on the

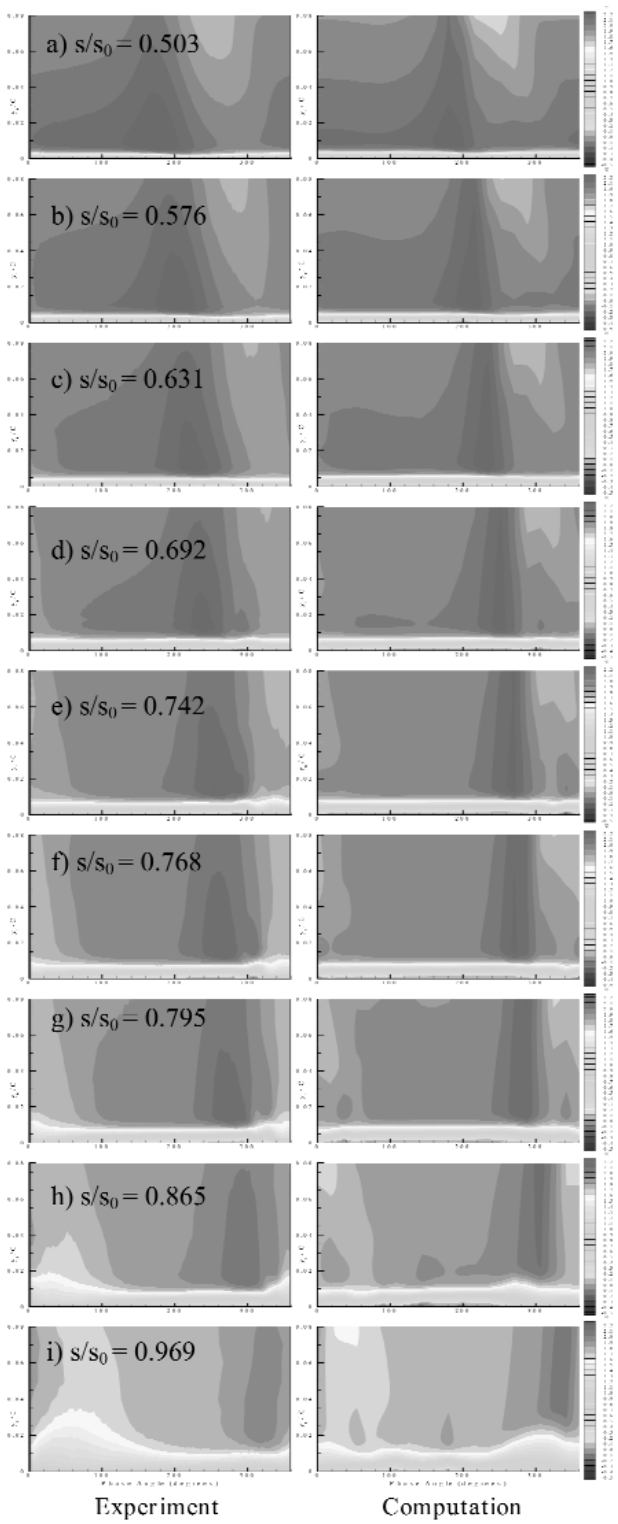


Figure 28. Comparison of computed and experimental velocity distributions at various streamwise station on suction surface of the blade for experiments of Stieger[22]. Horizontal axis: phase angle (0 to 360 degrees). Vertical axis: wall normal distance y_n/C (0 to 0·08). Contour levels: –0·5 to 2·2.

boundary-layer momentum thickness and streamwise distance limits its extension to three dimensional applications and unstructured grids, the success of the intermittency model and the accompanying

https://doi.org/10.1017/S0001924000000610 Published online by Cambridge University Press

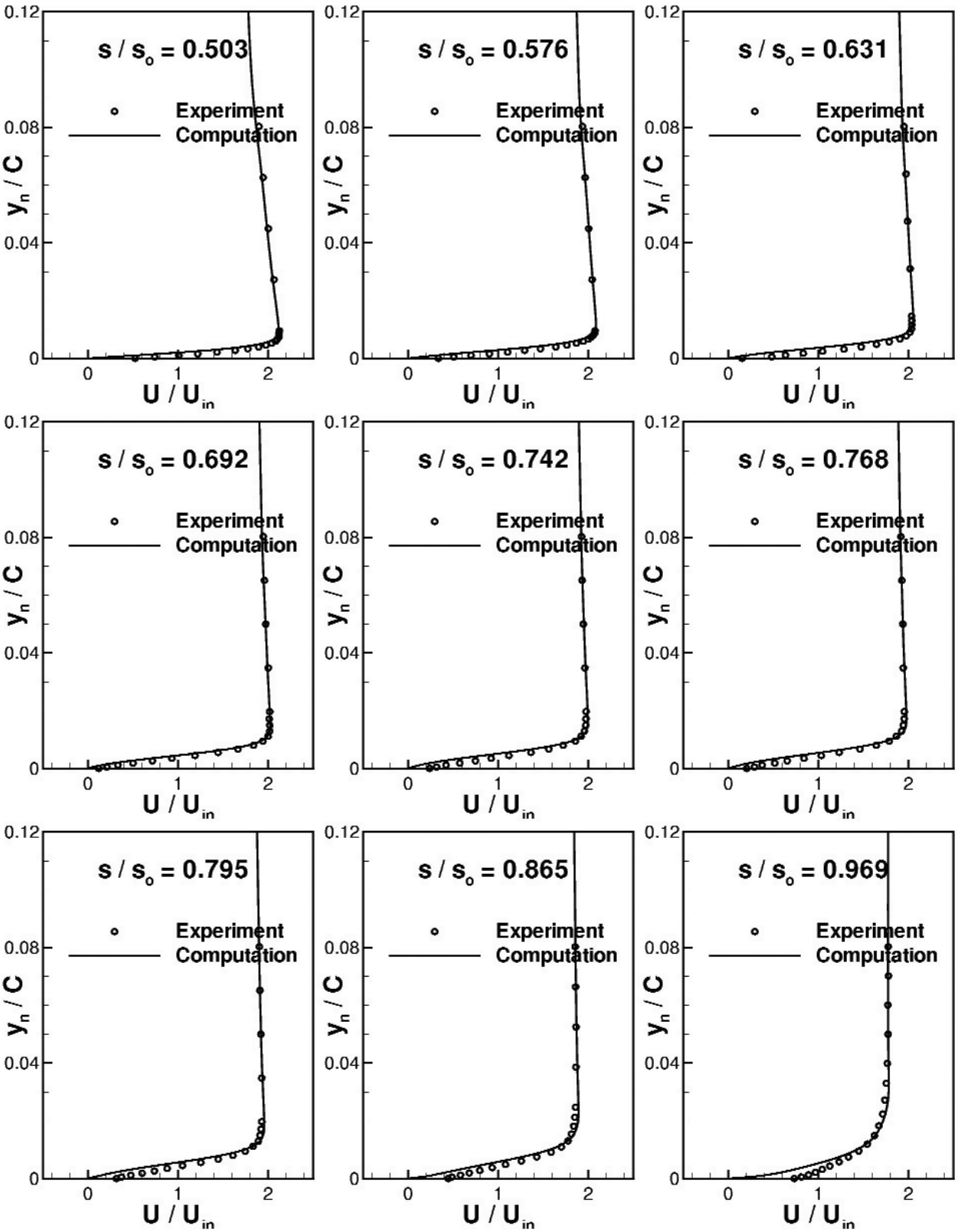


Figure 29. Comparison of computational and experimental mean velocity profiles at various streamwise locations on the suction surface of the blade for experiments of Stieger[22].

https://doi.org/10.1017/S0001924000000610 Published online by Cambridge University Press

correlations in accurately predicting transitional low-pressure turbine flows under diverse conditions has proven that the intermittency transport modelling approach provides an accurate and practical computational tool for transitional flow simulations. The success of the model and in particular the intermittency transport modelling approach for two dimensional flow computations has been instrumental in development of a more advanced transition model by Menter *et al*[42] based on local variables which does not have the limitations of the current model and readily applicable to three dimensional simulations and unstructured grids.

ACKNOWLEDGEMENTS

This work is supported by NASA Glenn Research Center under grant NCC3-590 and followed by grant NCC3-1040. The project is part of the low pressure turbine flow physics program of NASA-Glenn. We like to thank Dr David Ashpis for his coordination of the LPT effort. We would also like to thank Drs Terrence W. Simon, Richard W. Kaszeta, Ralph J. Volino, Thomas C. Corke, Flint O. Thomas, James P. Lake, and Paul I. King and Lennart S. Hultgren for providing their experimental data for this effort. The authors also appreciate Dr Howard Hodson's suggestion of T106 cascade experiments as a test case.

REFERENCES

1. MAYLE, R.E. The role of laminar-turbulent transition in gas turbine engines, *ASME J Turbomachinery*, 1991, **113**, pp 509-537.
2. RIVIR, R.B. Transition on turbine blades and cascades at low Reynolds numbers, 1996, AIAA Paper 96-2079.
3. LAKE, J.P., KING, P.I. and RIVIR, R.B. Low Reynolds number loss reduction on turbine blades with dimples and V-grooves, 2000, AIAA Paper 2000-0738.
4. SHARMA, O. Impact of Reynolds number on LP turbine performance, 1998, NASA/CP-1998-206958, pp 65-70.
5. SIMON, F.F. and STEPHENS, C.A. Modeling of the heat transfer in bypass transitional boundary-layer flows, 1991, NASA Technical Paper 3170.
6. DHAWAN, S. and NARASIMHA, R. Some properties of boundary layer during the transition from laminar to turbulent flow motion, *J Fluid Mechanics*, 1958, **3**, pp 418-436.
7. GOSTELOW, J.P., BLUNDEN, A.R. and WALKER, G.J. Effects of free-stream turbulence and adverse pressure gradients on boundary layer transition, *ASME J Turbomachinery*, 1994, **116**, pp 392-404.
8. SOLOMON, W.J., WALKER, G.J. and GOSTELOW, J.P. Transition length prediction for flows with rapidly changing pressure gradients, 1995, ASME Paper ASME-95-GT-241.
9. STEELANT, J. and DICK, E. Modelling of bypass transition with conditioned Navier-Stokes equations coupled to an intermittency transport equation, *Int J for Numerical Methods in Fluids*, 1996, **23**, pp 193-220.
10. CHO, J.R. and CHUNG, M.K. A k-ε-γ equation turbulence model, *J Fluid Mechanics*, 1992, **237**, pp 301-322.
11. DRIKAKIS, D. and GOLDBERG, U. Wall-distance-free turbulence models applied to incompressible flows, *Int J Computational Fluid Dynamics*, 1998, **10**, pp 241-253.
12. SUZEN, Y.B. and HUANG, P.G. Modelling of flow transition using an intermittency transport equation, 1999, NASA-CR-1999-209313.
13. SAVILL, A.M. Some recent progress in the turbulence modeling of by-pass transition, 1993, *Near-Wall Turbulent Flows*, SO, R.M.C., SPEZIALE, C.G. and LAUNDER, B.E. (Eds), pp 829-848, Elsevier Science.
14. SAVILL, A.M. Further progress in the turbulence modeling of by-pass transition, 1993, *Engineering Turbulence Modeling and Experiments 2*, RODI, W. and MARTELLI, F. (Eds), pp 583-592, Elsevier Science.
15. SIMON, T.W., QIU, S. and YUAN, K. Measurements in a transitional boundary layer under low-pressure turbine airfoil conditions, 2000, NASA-CR-2000-209957.
16. VOLINO, R.J. and HULTGREN, L.S. Measurements in separated and transitional boundary layers under low-pressure turbine airfoil conditions, 2000, ASME/IGTI Paper 2000-GT-0260.
17. LAKE, J.P., KING, P.I. and RIVIR, R.B. Reduction of separation losses on a turbine blade with low Reynolds number, 1999, AIAA Paper AIAA-99-0242.
18. HUANG, J., CORKE, T.C. and THOMAS, F.O. Plasma actuators for separation control of low pressure turbine blades, 2003, AIAA Paper No AIAA-2003-1027.
19. VOLINO, R.J. Separated flow transition under simulated low-pressure turbine airfoil conditions: Part 1- Mean flow and turbulence statistics, 2002, ASME Paper ASME-GT-30236.
20. KASZETA, R.W., SIMON, T.W. and ASHPIS, D.E. Experimental investigation of transition to turbulence as affected by passing wakes, 2001, ASME Paper 2001-GT-0195.
21. KASZETA, R.W., SIMON, T.W., OTTAVIANI, F. and JIANG, N. The influence of wake passing frequency and elevated free stream turbulence intensity on transition in low-pressure turbines, 2003, AIAA Paper AIAA-2003-3633.
22. STIEGER, R.D. The Effects of Wakes on Separating Boundary Layers in Low-pressure Turbines, 2002, PhD dissertation, Cambridge University, Engineering Department.
23. SUZEN, Y.B. and HUANG, P.G. Modeling of flow transition using an intermittency transport equation, 2000, AIAA Paper AIAA-2000-0287.
24. SUZEN, Y.B. and HUANG, P.G. Modeling of flow transition using an intermittency transport equation, *J Fluids Eng*, 2000, **122**, pp 273-284.
25. SUZEN, Y.B. and HUANG, P.G. Numerical simulation of transitional flows as affected by passing wakes, 2004, AIAA Paper AIAA-2004-0103.
26. SUZEN, Y.B., XIONG, G. and HUANG, P.G. Predictions of transitional flows in low-pressure turbines using an intermittency transport equation, 2000, AIAA Paper AIAA-2000-2654.
27. SUZEN, Y.B. and HUANG, P.G., HULTGREN, L.S., ASHPIS, D.E. Predictions of separated and transitional boundary layers under low-pressure turbine airfoil conditions using an intermittency transport equation, 2001, AIAA Paper AIAA-2001-0446.
28. SUZEN, Y.B., XIONG, G. and HUANG, P.G. Predictions of transitional flows in low-pressure turbines using an intermittency transport equation, *AIAA J*, 2002, **40**, (2), pp 254-266.
29. SUZEN, Y.B., HUANG, P.G., HULTGREN, L.S. and ASHPIS, D.E. Predictions of separated and transitional boundary layers under low-pressure turbine airfoil conditions using an intermittency transport equation, *ASME J Turbomachinery*, 2003, **125**, pp 455-464.
30. SUZEN, Y.B., HUANG, P.G., VOLINO, R.J., CORKE, T.C., THOMAS, F.O., HUANG, J., LAKE, J.P. and KING, P.I. A comprehensive CFD study of transitional flows in low-pressure turbines under a wide range of operating conditions, 2003, AIAA Paper AIAA-2003-3591.
31. MENTER, F.R. Two-equation eddy-viscosity turbulence models for engineering applications, *AIAA J*, 1994, **32**, (8), pp 1598-1605.
32. ABU-GHANNAM, B.J. and SHAW, R. Natural transition of boundary layers-The effects of turbulence, pressure gradient, and flow history, *J Mech Eng Sci*, 1980, **22**, (5), pp 213-228.
33. DAVIS, R.L., CARTER, J.E. and RESHOTKO, E. Analysis of transitional separation bubbles on infinite swept wings, *AIAA J*, 1987, **25**, (3), pp 421-428.
34. HUANG, P.G. and COAKLEY, T.J. An implicit Navier-Stokes code for turbulent flow modeling, 1992, AIAA Paper AIAA-92-0547.
35. RHIE, C.M. and CHOW, W.L. Numerical study of the turbulent flow past an airfoil with trailing edge separation, *AIAA J*, 1983, **21**, pp 1525-1532.
36. LAUNDER, B.E. and SHARMA, B.I. Application of the energy dissipation model of turbulence to the calculation of flow near a spinning disc, Letters in *Heat and Mass Transfer*, 1974, **1**, pp 131-138.
37. HSU, M.C., VOGIATZIS, K. and HUANG, P.G. Validation and implementation of advanced turbulence models in swirling and separated flows, 2003, AIAA Paper AIAA 2003-0766.
38. QUI, S. and SIMON, T.W. An experimental investigation of transition as applied to low pressure turbine suction surface flows, 1997, ASME Paper 97-GT-455.
39. JIANG, N. and SIMON, T.W. The influence of unsteady acceleration and turbulence intensity on transition in low-pressure turbines, 2003, AIAA Paper AIAA-2003-3630.
40. JIANG, N. and SIMON, T.W. Modeling laminar-to-turbulent transition in a low-pressure turbine flow which is unsteady due to passing wakes: Part I, Transition onset, 2003, ASME Paper ASME-GT2003-38787.
41. JIANG, N. and SIMON, T.W. Modeling laminar-to-turbulent transition in a low-pressure turbine flow which is unsteady due to passing wakes: Part II, Transition path, 2003, ASME Paper ASME-GT2003-38963.
42. MENTER, F.R., LANGTRY, R.B., LIKKI, S.R., SUZEN, Y.B., HUANG, P.G. and VOELKER, S. A correlation based transition model using local variables Part I — Model formulation, 2004, ASME Paper ASME-GT2004-53452.

https://doi.org/10.1017/S0001924000000610 Published online by Cambridge University Press